2 mil

PRECEDING PAGE BLANK NOT FILMED

Abstract

A specific need for low data rate communication study arises in the small probe communication link in deep space missions. The low available transmitter power and the large frequency uncertainty constrain the data rate to be low. An all-digital communication receiver is proposed and its feasibility is established. Although coherent systems should be used whenever practical, the noncoherent MFSK system is more suitable for very low data rates. The effect of Rician fading on the performance of MFSK receiver is studied. Fading characteristics of the Venus channel are examined based on the exponential model and available experimental data on the Venus atmosphere. Because of the requirement of high communication efficiency, three concatenated codes are evaluated and compared. The rapidly varying phase error at low data rate has great effects on the tracking loop behaviors which are examined by extensive computer study of the phase plane trajectories. Other topics discussed in this report include the spectrum of split-phase FSK and the coding/modulation selection for Pioneer-Venus communication systems.

Acknowledgement

The author would like to thank R.L. Kutz and Dr. R.W. Rochelle of NASA Goddard Space Flight Center for their continued encouragement and many valuable discussions throughout the work of this project; M. Fan, our research assistant, for significant contributions to Chapters 2 and 7; and Dr. W.C. Lindsey for encouragement and the review of several technical reports prepared for the grant. The financial support (grant) of NASA Goddard Space Flight Center on this project is gratefully acknowledged.

Chapter I Introduction

The exploration of the surface of the near planets via landers as well as flyby missions toward the far planets will, for at least the next decade, be restricted due to the weight limitations and the amount of electrical power available. As a result, the use of high power transmitters operating in conjunction with a directional antenna may not be possible. Thus the power level of telemetry signals received on earth will usually be below that necessary to perform coherent detection. The bit rate is low due to the power requirements.

As a possible solution to the problem, the use of M-ary noncoherent FSK has been considered for application in low-power space communications. Several forms of spectrum analyzer receivers have been proposed [1,2,3] to perform optimal detection in the presence of large frequency uncertainty caused largely by doppler shifts and the oscillator instability. The problems of time and frequency synchronizations have been analyzed [4]. And for specific multipath models, the effects of multipath on the communication system performance have been examined [5,6].

With the advent of digital hardware, a practical implementation of the M-ary noncoherent FSK is the use of the fast Fourier transform (FFT) receiver. In the ideal case the FFT receiver should perform exactly the same as the optimum noncoherent MFSK receiver. The system operation at low data rate allows the use of sophisticated signal processsing. The performance of the digital system, however, is limited by the effects of quantization and finite word length. These problems are examined in Chapter 2. Theoretical performance of the optimum noncoherent MFSK receiver with and without multipath fading is considered in Chapter 3. For the "Rician" channel model assumed, it is found that for a given average error probability, the required increase in the energy-to-noise density ratio to combat the multipath fading is reasonably small, particularly when the bit duration-IF filter bandwidth product is large.

One important application of the low data rate communications is the Pioneer Venus communication link. The dense Venus atmosphere causes a severe fading on the communication link between the descending atmospheric entry probe and the Earth. The most important atmospheric effect is due to the turbulence in the Venus atmosphere. Based on the latest Venus 7 and Venus 8 data, we may conclude now that fading effect is not as severe as early predictions based on the Venus 4 data. In Chapter 4, we examine the following problems: the probability of different fading levels relative to the free space as a function of altitude, the fading rate, the autocorrelation function and the spectrum of amplitude and phase variations, and the spectrum spreading due to turbulence. An exponential turbulence model proposed by DeWolf [7] is used in the analysis. It is believed that the turbulent Venus atmosphere will not cause serious communication problem in the forthcoming Pioneer Venus mission.

The capacity of the M-ary noncoherent channel is, however, very limited especially at low signal-to-noise ratio [8]. Additional coding implemented by concatenating the inner code and the outer code can provide low error rate without excessive decoding complexity. Performance of three different concatenated coding techniques is studied in Chapter 5. The split-phase baseband format has become increasingly important. In Chapter 6, the spectrum of the modulated signals with split-phase baseband is examined. The discussion of this chapter clarifies the ambiguities among all available results [9].

The performance of command and telemetry systems, useful in deep-space communications, is frequently affected by the radio-frequency phase error which is introduced at the point of reception by means of the carrier tracking loop. In low data rate communications, the phase error may vary rapidly over the duration of a signalling interval. If the input phase is varying according to a polynomial function of time, then the phase error can be reduced to zero in steady state by

using higher order loops. Exactly how the phase error is varying in time is not known. One way to model the phase variation is to assume that it be a sinusoidal function of time. Extensive computer analysis of the phase-plane trajectories has shown that there are threshold values for both the frequency and amplitude of such sinusoidal variation. This is the subject of Chapter 7.

In Chapter 8, we consider different candidates for coding and modulation and the interplex system which provides a coherent system without relying on the perfect reference signal. Finally in Chapter 9, the conclusions and recommendations for further study is presented.

Chapter II The Fast Fourier Transform Receiver

I. Introduction

The advent of large scale integration has suggested a new approach to signal processing problems. In the design of communication receivers, the trend has been toward the increased use of digital circuitries. The speed of the present digital hardware, however, has prevented the data rate from being in the range of gegabits per second. For low data rate communication such as between 1 kilobits per second to 1 bit per second or lower, the digitial system is not only technically feasible, but also has potential cost reduction over the existing receiving systems. The low data rate communication system we consider here is designed primarily for deep space communications. It is also suitable for other applications as long as the data rate is reasonably low. The digital filters employed in the system can operate fast enough so that it may be time-shared among a number of channels.

For deep space applications, such as the communication between the earth and a probe in the atmosphere of Venus, the small transmitter power of the probe has constrained the data rate to be low. The large frequency uncertainty caused primarily by the oscillator instability and the doppler effects requires a large IF filter bandwidth and thus the received signal-to-noise ratio is very small. To have an efficient communication, it is necessary to remove such frequency uncertainty. A small amount of frequency error which cannot be removed may be tracked by an automatic frequency control (AFC) loop. In this chapter we propose a fast Fourier transformer receiver where all components are implemented digitally except the frequency down conversion. To perform the mixing operation at 2.3 GHz, the typical operating frequency, by using digital circuitry is not feasible at the present time. Correlation operation in the kilo-hertz frequency range, however, can easily be performed digitally.

There are practical limitations on the digital systems. For example, the computer word length is finite and the A/D conversion error and the round off error are unavoidable. Such limitations will be examined in detail.

II. System Configuration and the FFT Operation

The propsed system is shown in Fig. 1. With the exception of the frequency down conversion and the local oscillator, the receiving system can be implemented digitally. The input to the A/D converter can have a frequency of several hundred hertz to a few thousand hertz depending on signalling frequency and the uncompensated frequency uncertainty due to oscillator instability and doppler frequency variations. The sampling rate should be at least twice of the largest frequency of the input signal. Experience has indicated that the desirable sampling rate be four or five times of the signal frequency. The digitized data may be recorded in magnetic tape to guard against the loss of data due to system failure such as loss of lock in time or frequency synchronization. Digital filtering of the digitized data reduces the noise in the received signal. This operation is optional if the signal-to-noise ratio is high but is essential if the signal-to-noise ratio is low. The discrete Fourier transform (DFT) of the data is performed by using the fast Fourier transform (FFT). The square of the magnitude of DFT is proportional to the power spectrum. The decision is based on the frequency of the largest spectral component. In the absence of noise, the receiver will always select the correct frequency. However, the magnitude of the measured spectral peak depends on the word timing error. In the presence of noise, time sync. loop provides the word tracking. The frequency sync. loop determines the frequency drift and provides an up-to-date estimate of the actual frequency. The local oscillator frequency can then be adjusted according to the frequency estimate. As the data rate is low, there is sufficient time for on-line, i.e. real-time, operation of the complete system to provide continuous frequency and time tracking and the signal-to-noise ratio improvement via digital filtering.

The fast Fourier spectral analysis can be very sensitive to the signal-to-noise ratio. Consider two FSK signals of frequencies 100 Hz and 200 Hz. Each bit of the received data contains one of the two signals plus an additive Gaussian noise. The bit duration is 1 sec. and the sampling rate is 1000 samples per second. The bit duration - IF filter bandwidth product is thus equal to 100. For signal-to-noise ratios $(S/N)_i = 0.1$ and 0.01, Figures 2 and 3 show the power spectra of a FSK signal plus noise. All spectral peaks are detected correctly in the signal-to-noise ratios considered. To avoid possible false spectral peaks which cause decision errors, it may be necessary to do some signal processing to increase the signal-to-noise ratio. By doubling the sampling rate we can use twice as many signal samples per spectrum. The adjacent points in the power spectrum can be averaged to give [1],

$$P(n) = \left|\frac{1}{N} \sum_{i=0}^{2N-1} x_i \exp\left(-j \frac{\pi}{N} in\right)\right|^2 + \left|\frac{1}{N} \sum_{i=1}^{2N-1} x_i \exp\left[-j \frac{\pi}{N} i(n+1)\right]\right|^2, \qquad n = 0, 2, 4, \ldots, N \tag{2.1}$$

Figure 4 shows the power spectra of the "two-point" averages given by Eq. (2.1). Very little is changed in the spectral peaks but the noise is smoothed somewhat. Increasing the number of averaged points to, say, 4 and 10 may not have the desired improvement. This is illustrated in Figure 5 for $(S/N)_i = 0.1$ and Figure 6 for $(S/N)_i = 0.01$. It appears that 4 is the maximum number of points that can be averaged to obtain any meaningful improvement from spectral averaging. Other considerations of the spectral averaging have been given by Winkelstein [10]. The use of digital bandpass filtering can also improve the power spectrum.

The FFT receiver usually has more difficulty to detect the highest signal frequency component unless the sampling rate is much higher than such frequency ([3]; The signal-to-noise ratios in Ref. 3 should be divided by a factor of 2). In spite of some practical problems with the FFT receiver as described above, the use of sophisticated signal processing at low data rate makes the FFT receiver a

very feasible system for deep space communications. Furthermore, the FFT hardware presently available has a speed several times faster than the use of FFT software. Such improvment in processing time from using digital devices is particularly important for real-time applications.

The probability of error of the fast Fourier transform receiver is the same as the optimum noncoherent MFSK (multiple frequency shift keyed) receiver. If sampling, quantization and finite word length effects are considered, the performance will no longer be optimum. The sampling rate can always be chosen to be large enough to have negligible effects. Quantization and finite word length effects may seriously limit the use of the FFT operation. These problems will be discussed later.

III. Frequency Tracking in the MFSK Receivers

A large amount of frequency drifts that cause uncertainty may be removed by prior knowledge and prediction. However, other drifts will surely remain, and it is necessary to track these in any practical system. Several techniques of frequency tracking have been proposed. Goldstein's technique [1] obtains a frequency discriminator characteristic (S curve) by taking the difference, F_n, of the two terms in Eq. (2.1) as an estimate of the current frequency error,

$$F_n = r_{n+1} - r_n \tag{2.2}$$

where

$$r_n = \left| \frac{1}{N} \sum_{i=0}^{2N-1} x_i \exp\left(- j \frac{\pi}{N} in\right) \right|^2$$

is the nth spectral line. Let T be the signal duration. The nominal signal frequency here is $(n + \frac{1}{2})/T$, centered between two adjacent spectral lines. F_n is filtered and used to correct the local oscillator tuning as in any frequency-locked loop. The procedure is simple as it involves only FFT. One practical problem, however, is that F_n is not necessarily equal to zero even if there is no frequency

drift and no noise. Furthermore the method is suitable for very small frequency drift which may not be the case in practice.

The second technique due to Ferguson [2] is to use a weighted average of the k closest spectral components, where k is some small integer. If the received signal is norminally at frequency n/T, then the estimate is

$$F_n = C \sum_{i=k-k/2}^{k/2} a_i r_{n+i} \tag{2.3}$$

where C is a normalizing constant and the a_i's are a set of linearizing weighting coefficients. This technique of course is highly dependent on the choice of the a_i's.

The third technique due to Chadwick[11] is based on the spectral lines nearest to the observed frequency. Let r_o be the spectral component of the observed frequency and r_{+1} and r_{-1} be the adjacent spectral lines with frequency 1/T Hz larger and smaller, respectively, than the observed frequency. The frequency estimate is

$$F_n = \frac{r_{+1} - r_{-1}}{2r_o T} \tag{2.4}$$

which tends to have less accuracy than Eq. (2.3) and is useful only to very small frequency drifts.

The fourth technique due to Simon [12] is an improvement of the third technique. The frequency estimate proposed by Chadwick and used in a closed loop tracker suffers from the fact that it is biased. In fact Simon [12] was able to prove that a frequency estimator based on spectral estimates taken at integer multiples of 1/T cannot be unbiased. To be unbiased, the conditional mean of the frequency estimate must have the linear variation. It turns out that all frequency estimators made up of spectral estimates taken at multiples of 1/T have a conitional mean which has zero slope at the origin. Simon proposed an estimator which is derived

from spectral estimates taken at the adjacent 1/2T points. His estimate is

$$F_n = \frac{r_{+\frac{1}{2}} - r_{-\frac{1}{2}}}{2(r_{+\frac{1}{2}} + r_{-\frac{1}{2}})} \tag{2.5}$$

Although this requires a slight increase in spectral computation, the variation of the conditional mean of this estimator is linear in the neighborhood of the origin and thus presents a better estimator for constructing a closed loop frequency tracking algorithm.

The fifth technique digitally implements the automatic frequency control loop for frequency tracking (See Fig. 1). Detail discussion of the digital AFC loop is given in Ref. 2 where it is shown that the variance of the frequency estimate is smaller than that of Eq. (2.4). The time sync. loop can be implemented digitally in a similar manner as the AFC loop.

IV. Effects of Quantization and Finite Word Length

The A/D (analog to digital) conversion error and the round-off error of the digital AFC loop are described in Ref. 3. It is shown that a commercially available 14 bit register length is adequate to provide a signal-to-noise ratio of over 40 dB in digital filtering.

The round-off noise has a more serious effect in the FFT operation. Let E_o be the quantization interval. For N-point FFT, the round-off noise variance with fixed point arithmetic is given by [13]

$$\sigma_E^2 \approx 4N \left(\frac{E_o^2}{12} \right) \tag{2.6}$$

which is proportional to N. The variance can be reduced by scaling, such as the multiplication factor of 1/2, at each stage of the FFT operation. Scaling, of course, requires a slight increase in the digital hardware. With scaling, the variance becomes

$$\sigma_E^2 = 20 \left(\frac{E_o^2}{12} \right) \tag{2.7}$$

but the noise-to-signal ratio is $5NE_o^2$ which is still proportional to N. In low data rate communication, a typical value for N is 1024. To achieve a signal-to-noise ratio of 40 dB, the required register length is 13 bits. If the siganl dynamic range is also considered, much longer register length is needed. Thus the number of points that can effectively be performed by a given FFT hardware or software is limited. If the floating-point arithmetic is used, the mean square error (round-off noise variance) is upper bounded by [14]

$$\sigma_E^2 \leq 3m\left(\frac{E_o^2}{3}\right) \tag{2.8}$$

where $N = 2^m$ is a power of 2. For N = 1024, the variance given by Eq. (2.8) is greater than that of Eq. (2.7) but smaller than that of Eq. (2.6).

V. Concluding Remarks

With the present technology in digital devices, we have shown that the proposed all-digital low data rate communication system which employs a fast Fourier transform receiver is completely feasible from both performance and economy viewpoints. The effects of the quantization and finite word length on the digital system performance are normally very significant. It is shown in this chapter, however, that by properly designing the digital filters and implementing the FFT operation, such effects can be minimized. A commercially available 14 bit register length can provide a signal-to-noise ratio of over 40 dB in both digital filtering and FFT. With continued improvement in the digital hardwares, there is every reason to believe that the proposed all-digital system provides cost-reduction over existing receiver systems.

Chapter III Performance of Wideband Noncoherent MFSK System with Multipath Fading

I. Introduction

Reports from the Mariner V S-band measurements [15], [16] and the Soviet Space Probe Venera 4, 5 and 6 have both indicated the severe fading of radio signals at the turbulent Venus atmosphere. Refraction of the radio beam by the charged particles of the upper atmosphere and the gases that constitute the lower atmosphere produce changes in frequency, phase and amplitude of the signal received at the deep-space tracking stations on the Earth. In addition, the amplitude of this signal was affected both by defocusing and absorption in the lower atmosphere. It is necessary to consider the performance of the noncoherent coded system under various fading conditions. Glenn [17], Schuman [18], and Chadwick [5] have examined the effects of multipath fading on the low data rate communications. Their results, however, are inconsistent and limited to the wideband binary FSK. The Gaussian assumption made by Glenn for very large IF filter bandwidth (b_oHz) and bit-duration (T_b) product may not be valid for intermediate values of b_oT_b, say $1 < b_oT_b \leq 10$. In this chapter the exact error probability of the wideband noncoherent MFSK receiver is derived from using the well known "Rician" channel model [19]. The received signal consists of the specular and the random scatter (diffuse) components. The results correspond to the situation that the reflected siganl has a much larger bandwidth then the direct signal and that the time delay between the direct and the reflected signals is much less than the bit duration. This represents the most important kind of multipath fading. Other multipath fading conditions that may limit the performance more but have a smaller probability of occurence are also considered. They are: (1) the reflected signal amplitude is assumed to be constant over a bit period but varies randomly according to the Rayleigh distribution from bit to bit, and (2) the delay of the reflected signal exceeds one bit period. The reflected signal may then be considered as part of the additive noise.

II. Error Probability Computation

Consider a noncoherent MFSK receiver which has 2^n parallel channels where n is the number of information bits per word. In the absence of multipath fading, the probability density of the output of the kth channel which is mateched to the kth signal input is [20]

$$p(x_k) = \frac{1}{2N_o b_o T_b} \exp - \left(\frac{x_k + 2nE}{2N_o b_o T_b} \right) I_o \left(\frac{\sqrt{2nEx_k}}{N_o b_o T_b} \right); \; x_k > 0 \qquad (3.1)$$

$$= 0 \quad \text{otherwise}$$

where E is the signal energy per bit. For $b_o T_b = 1$, and with multipath fading, Lindsey [21] has shown that

$$p(x_k) = \frac{1}{1 + \beta} \exp - \left[\frac{x_k + \rho}{1 + \beta} \right] I_o \left[\sqrt{\frac{4\rho x_k}{(1 + \beta)^2}} \right]; \; x_k > 0 \qquad (3.2)$$

$$= 0 \quad \text{otherwise}$$

and the probability density of the output from other channels which are not matched to the kth signal is

$$p(y_i) = p(y) = \exp(-y); \; y > 0 \quad \Big\} \; j \neq k$$

$$= 0 \quad \text{otherwise} \quad \Big\}$$

The parameters ρ and β in Eq. (3.2) are, respectively, n times the energy-to-noise ratio per bit of transmitted information produced by the specular component and n times the energy-to-noise ratio per bit of transmitted information produced by the scatter component, i.e.

$$\rho = n\left(\frac{\alpha^2 E}{N_o} \right); \quad \beta = n\left(\frac{2\sigma^2 E}{N_o} \right) \qquad (3.4)$$

where α is a factor proportional to the strength of the specular component and σ^2 is the variance of the scatter component. By comparing Eqs. (3.1) and (3.2), with $b_o T_b = 1$, we note that in going from "no fading" to "with fading", the following change is made:

$$\frac{E}{N_o} \rightarrow \frac{E}{N_o} \frac{\alpha^2}{1 + \beta}; \; x_k \rightarrow x_k \frac{1}{1 + \beta}$$

By using the transformation $x = x_k \frac{(1+\beta)}{2N_o}$ and multiplying E/N_o by $\alpha^2/(1+\beta)$, Eq. (3.2) becomes

$$p(x) = \frac{1}{(1+\beta)b_o T_b} \exp - \left[\frac{x+\rho}{(1+\beta)b_o T_b}\right] \quad I_o \left[\frac{4\rho x}{(1+\beta)b_o T_b}\right] ; \; x > 0$$
$$= 0 \quad \text{otherwise} \tag{3.5}$$

At the output of the kth channel, the sample average of $M = b_o T_b$ samples is denoted as u. The characteristic function of u is

$$\phi(t) = \frac{1}{[1 - i(1+\beta)t]^M} \exp - \left[\frac{nE}{N_o} \frac{\alpha^2}{1+\beta} \left(1 - \frac{1}{1 - i(1+\beta)t}\right)\right] \tag{3.6}$$

Similarly the sample average v of M samples in other channels has the characteristic function

$$\phi(t) = \frac{1}{(1 - it)^M} \tag{3.7}$$

The probability densities p(u) and p(v) can be determined from Eqs. (3.6) and (3.7) respectively. The exact error probability is

$$P_E(n) = 1 - \int_o^\infty p(u)du \left[\prod_{j=1}^{2^n-1} \int_o^u p(v_j)dv_j\right]$$
$$= 1 - \int_o^\infty e^{-(u + \frac{nE}{N_o} \frac{\alpha^2}{1+\beta})} \frac{I_{M-1}\left(2\sqrt{\frac{nE}{N_o}\frac{\alpha^2}{1+\beta}\,u}\right)}{\left(\sqrt{\frac{nE}{N_o}\frac{\alpha^2}{1+\beta}}\right)^{M-1}} u^{\frac{(M-1)}{2}} \left[\frac{1}{(M-1)!} \int_o^{u(1+\beta)} v^{M-1} e^{-v} dv\right]^{2^n-1} du \tag{3.8}$$

Equation (3.8) is consistent with Lindsey's result [21] for M = 1 and Chen's result [20] for no fading case ($\beta = 0$, $\alpha = 1$),

$$P_E(n) = 1 - \int_o^\infty e^{-(u+\frac{nE}{N_o})} u^{M-1} \frac{I_{M-1}\left(2\sqrt{\frac{nEu}{N_o}}\right)}{\left(\sqrt{\frac{nEu}{N_o}}\right)^{M-1}} \left[\frac{1}{(M-1)!} \int_o^u v^{M-1} e^{-v} dv\right]^{2^n-1} du \tag{3.9}$$

where

$$\frac{1}{(M-1)!} \int_o^u e^{-v} v^{M-1} dv = 1 - e^{-u} \sum_{k=0}^{M-1} \frac{u^{M-k-1}}{(M-k-1)!}$$

A listing of computer programs to calculate Eq. (3.8) is given as Appendix of this chapter. Equation (3.8) is also similar to an error probability expression derived by Lindsey ([22], Eqs. (37) and (33)). Accurate computation of the integral in the Lindsey's expression has recently been made by Adams [23], which is adapted to the computation* of Eq. (3.8). For M = 5, 10, and 100 with N = 4 and 64, the error probabilities are plotted in Figs. 7, 8, 9 respectively, versus the total average received signal energy per bit to noise density ratio,

$$(1 + \gamma^2)\beta/n = (\alpha^2 + 2\sigma^2)E/N_o \tag{3.10}$$

for $\gamma^2 = 0,1,10$, and $10^5(\infty)$. For $\gamma^2 = \infty$, $(1 + \gamma^2)\beta/n = E/N_o$. It is interesting to note that for communication channels which are largely scatter in nature, i.e. $\gamma^2 < 2$, the error performance improves as M increases for large E/N_o. Also the performance degradation due to multipath fading decreases as M becomes large. This is probably due to the fact that the MFSK receiver is a noncoherent energy detector and the reflected signal tends to increase the total signal energy.

III. Other Multipath Fading Conditions

The above results are based on two assumptions: (1) the reflected signal is purely random and the direct signal contributes to the nonrandom (specular) component of the received data, and (2) the reflected signal has a negligible time delay from the direct signal. The second assumption is clearly justified in view of the vast communication distance involved. The first assumption holds when the altitude of the space probe above the Venus surface is large enough that the Venus atmosphere has little effect on the direct signal.

---

*The author would like to thank Dr. Lindsey for calling his attention to the computer program prepared by W.B. Adams, and Mr. Adams for using his computer program [23].

If the second assumption is not satisfied, the reflected signal may not be received at the same bit duration as the direct signal. Consider the worst case that the reflected signal provides no information and can be included in the additive noise. Then the average received energy-to-noise density ratio per information bit is

$$\frac{\alpha^2 E}{2\sigma^2 E + N_o} = \frac{\gamma^2}{1 + \frac{n}{\beta}} \tag{3.11}$$

That is the total received energy-to-noise density ratio per bit is reduced by a factor

$$\frac{(1 + \gamma^2)(1 + \beta/n)}{\gamma^2} \geq 1; \quad \gamma^2 \neq 0 \tag{3.12}$$

The error probability given by Eq. (3.8) is still valid if the required increase given by Eq. (3.12) is taken into account in plotting the error probability. For $\gamma^2 = 0$, then the receiver does not receive any useful information and the probability of error is $1 - 1/N$. As β increases, Eq. (3.12) indicates that the required increase in the energy-to-noise density ratio is almost a linear function of β.

Next we consider the case that the first assumption is not valid. The reflected signal is now assumed to be constant over a bit period but varies randomly according to the Rayleigh distribution from bit to bit. Furthermore, the time delay of the reflected signal is assumed to be negligible. The error probability can be derived as follows. First obtain the error probability without fading by setting $\beta = 0$ and $\alpha = 1$ in Eq. (3.8). Consider now $S = E/T_b$ as a random variable with Rician distribution,

$$p(S) = \frac{1}{2\sigma^2} \exp\left[-\frac{1}{2\sigma^2}(S + S_b)\right] I_o\left[\frac{\sqrt{SS_b}}{\sigma^2}\right] \tag{3.13}$$

where S_b is the power of the direct signal component. The error probability without fading is then multiplied by Eq. (3.13) and integrated with respect to S from 0 to ∞.

In conclusion, it is remarked that multipath fading is an important consideration in the forthcoming deep space missions. An accurate evaluation of the multipath fading effect requires a realistic channel model which has to be derived from the experimental results. As severe fading occurs only for a short period of the entire mission, the percentile error probability must also be computed.

Chapter IV Atmospheric Effects on Pioneer Venus Communication Links

I. Introduction

Based on the communication signals received from Venera 4, 5, 6 and 7, there is definitely observed fading which may be caused by turbulence in the Venus atmosphere. In order to determine the possible effects that turbulence could have on an S-band communication system, theoretical studies have been made [7, 22, 23, 24, 25, 26] to compare with the limited experimental data available. Assumption was made in these studies that the observed effects were indeed due to turbulence. It was recognized, however, that other factors such as absorption, refraction and defocusing, and the unexplained motion of the probe, may also contribute to the observed fading. But since turbulence appears to play the dominant role, it is necessary to see what type of S-band effects might produce, and the implications of these effects on the S-band communication systems.

Venera-7 data indicates that there is no fading at 1 GHz with radio waves propagating vertically through the entire thickness of the Venus atmosphere. Fading is still severe as the space probe traversed the planet's atmosphere. These conclusions are not consistent with the earlier results from Venera-4 data. Venera-7 data should be more reliable, however, as the probes did land on the Venus surface. Additional reports on turbulence effects and Venera-7 data are available in Refs. 27-31. Reference 27 is particularly informative on Venera-7 data. A summary of U.S. efforts on Venus study is given by Ref. 32.

Along with the limited experimental data, theoretical studies are useful to draw meaningful conclusions of the turbulence effects on radio wave propagation through the Venus atmosphere. The book by Tatarski [33] provides a useful background for the study. The theoretical problem areas to be studied are as follows:

1. The probability of different fading levels relative to free space as a function of altitude.

2. The fading rate, i.e. the number of fades per second.
3. The autocorrelation function of the amplitude fluctuations about the mean value.
4. The autocorrelation function of the phase fluctuations about the mean value.
5. The phase and frequency spectra.
6. The spectrum of the frequency fluctuation about the carrier frequency, i.e. the spectrum spreading due to turbulence.

II. Fading Levels

Fig. 10 shows the geometry assumed for the propagation problem. The procedure for calculating fading levels is as follows.

The fading of Venera-4 as a function of altitude can be approximated by [26],

$$\sigma_A(z,\ 0.94\ \text{GHz},\ \theta = 0^\circ) = 1.175 \exp(-\ 0.0785\ z) \tag{4.1}$$

over the 20-40 Km altitude range, where

$$\sigma_A^2 = \frac{\langle A^2 \rangle - \langle A \rangle^2}{\langle A \rangle^2} \tag{4.2}$$

A is the signal amplitude, z is the height above the Venus surface, and $\langle \cdot \rangle$ denotes the time average. These measurements were taken at a frequency f = 0.94 GHz and at a sub-earth point, i.e. $\theta = 0^\circ$. Note that the scale height as defined by Eq. (4.1) is h = 1/0.0785 = 12.7 Km. When the frequency and θ are changed, scaling laws must be used to calculate σ_A. Under reasonable assumptions, the following [26] are two possible cases for scaling σ_A^2.

Case (a): $L_o \gg \sqrt{\frac{2\pi h\lambda}{\cos\theta}}$

$$\sigma_A^2 = \text{const.}\ \frac{k^2}{\cos\theta} \tag{4.3}$$

Case (b): $L_o \ll \sqrt{\frac{2\pi h\lambda}{\cos\theta}}$

$$\sigma_A^2 = \text{const.}\ \frac{k^{7/6}}{(\cos\theta)^{11/6}} \tag{4.4}$$

where L_o is the outer scale of turbulence, $k = 2\pi/\lambda$, and λ is the wavelength. Using the scaling laws (4.3) and (4.4) and Eq. (4.1), we find,

Case (a) $\sigma_A(z, 2.3\ \text{GHz}, \theta = 60^\circ) = 4.07 \exp(-0.0785\ z)$ (4.5)

Case (b) $\sigma_A(z, 2.3\ \text{GHz}, \theta = 60^\circ) = 3.74 \exp(-0.0785\ z)$ (4.6)

Given σ_A, the fading level distributions can be calculated assuming that the probability distribution of the amplitude scintillations is Rice-Nakagami (a constant vector plus a Rayleigh distributed vector). Based on DeWolf's formula [22], we let $\sigma_A = \sigma_\varepsilon$. The signal with electric field E(s) becomes a constant-plus-Rayleigh distributed vector, i.e.

$$E(s) = E_o(s)[\exp(-\sigma_\varepsilon^2) + \delta B] \tag{4.7}$$

where δB is Rayleigh distributed, with zero mean and $\langle|\delta B|^2\rangle = 1 - \exp(-2\sigma_\varepsilon^2)$. For σ_A or σ_ε calculated in (4.5) or (4.6), we can compute the Norton parameter K defined by DeWolf [22] as

$$K = 10 \log_{10}[\exp(2\sigma_\varepsilon^2) - 1] \tag{4.8}$$

which is the ratio of powers in the two terms of Eq. (4.7)

Using the formulas in Norton's paper [34], the probability of different fading levels may be found. A computer program which was originally prepared by Dr. Strohbehn was adapted here for the computation of the fading levels for various probabilities as a function of altitude. A listing of the computer programs for fading level computation is given as the Appendix to this chapter. Because of the uncertainty on L_o, both Eqs. (4.5) and (4.6) were used for scaling. For carrier frequency 2.3 GHz and $\theta = 60^\circ$, the two scaling laws provide essentially the same results. For probabilities less than 0.05, the fading level vs the altitude plots shown in Fig. 11 have dips at altitudes between 20 and 25 km for both scaling laws. The problem [35] is essentially due to the fact that equations for generating the

fading levels are polynomial approximations in the parameter k(k_1, k_2 in the computer printout). Since only a few terms are kept in the approximations, the results are very poor for k values close to unity. It is noted that the dips all occur between 20 and 25 km where the k value is going through unity. A simple curve fitting through this trobulesome region still provides accurate results. Fig. 12 is the fading level plot for various probabilities. The transition from p = 0.15 to p = 0.20 is not a smooth one; so two separate plots are provided in Fig. 12. Other fading level plots are given by Chen [36]and Strohbehn [26].

III. Fading Rates

Given that there may be strong fading, the next parameter of interest is the fading rates. In order to get a feel for the magnitude of this parameter, it was approached from several different directions. The first two estimates were based on the observed fading rate of 1 fade/sec. as measured by Venera-4 and reported by DeWolf [22]. In the first estimate, it is assumed that the fading rate will scale as

$$f_A(f_{C_2}) = \sqrt{\frac{f_{C_2}}{f_{C_1}}}\, f_A(f_{C_1}) \tag{4.9}$$

where f_A is the fading rate and f_{C_1} and f_{C_2} are the carrier frequencies. This formula assumes the fading is dominated by local winds. It gives a value of about 1.5 fades/sec. for a carrier frequency of 2.3 GHz. The second estimate assumes that the motion of interest is the velocity of the probe, and the scaling law becomes

$$f_A(f_{C_2}, v_2) = f_A(f_{C_1}, v_1)\, \frac{v_2}{v_1} \sqrt{\frac{f_{C_2}}{f_{C_1}}} \tag{4.10}$$

Again at 2.3 GHz, $f_A = 1.5\, v_2/v_1$ where v_2/v_1 is the ratio of the velocities of the new probe to the Venera probe.

The third estimate was made completely independently of the Venera-4 data. It is known from turbulence theory that the critical size of an inhomogeneity to produce fading is roughly,

$$L_C = \sqrt{\frac{\pi \lambda L}{8}} \qquad (4.11)$$

where L is the effective path length in the turbulent medium. The fading rate then is

$$f_A = \frac{v_p}{L_C} \qquad (4.12)$$

where v_p is the velocity of the probe perpendicular to the line-of-sight of the propagation path. For the case of interest here,

$$f_A = \frac{0.866\, v}{\sqrt{\frac{\pi \lambda L}{8}}} \qquad (4.13)$$

For λ = 15 cm, we get $f_A = 3.6\ v/\sqrt{L}$. If the probe is moving on the order of 30 m/sec in the lower part of the atmosphere, then we get f_A = 0.54 to 1.5 fades/sec. as the effective length, L, varies between 40 Km and 5 Km.

The above calculations give us a rough idea for the expected fading rates. A more sophisticated model can be used to predict the fading rate as a function of altitude by knowing the velocity of the probe and using an exponential model for the turbulent atmosphere.

For Venera-7, the vertical velocity before impact is 17 m/sec. The fading rate from Eq. (4.12) is 0.985 fade/sec. It may be concluded from the above discussion that the maximum fading rate is 1.5 fades/sec.

IV. Concluding Remarks

The autocorrelation functions of the amplitude and phase fluctuations, and the phase and frequency spectra and spectrum spreading are all described in detail in Refs. 26 and 36. It was shown that neither the pahse fluctuations nor the frequency spreading would be a major problem in system considerations. The very limited preliminary report available on the "Venus-8" data indicates that the data from "Venus-8" are similar to that from "Venus-7" [35].

It is reasonable to conclude that based on the Venera data and the exponential turbulence model proposed by DeWolf, there will always be strong fading at low altitude (below 20 km), particularly near the Venus surface. Fading is least significant if $\theta = 0^{\circ}$. Further study on the subject matter of this chapter is much needed, however, to assure the success of the forthcoming Pioneer-Venus mission.

Chapter V Concatenated Coding for Low Data Rate Communications

I. Introduction

In deep space communications with distant planets, the data rate as well as the operating signal-to-noise ratio may be very low. To maintain the error rate also at a very low level, it is necessary to use a sophisticated coding system (longer code) without excessive decoding complexity. The concatenated coding has been shown to meet such requirements in that the error rate decreases exponentially with the overall length of the code while the decoder complexity increases only algebraically. Three methods of concatenating an inner code with an outer code are considered. Performance comparison of the three concatenated codes is made. It is shown that the concatenated code with inner code a convolutional code and outer code a Reed-Solomon code performs the best among the three. Refs. 37-46 contain most of the available informations on the concatenated code. Performance of the concatenated codes in the presence of multipath fading has not been considered. This chapter is based on Ref. 47.

II. Concatenated Codes

The three concatenated codes considered are:

Code I. inner code a bi-orthogonal code, outer code a generalized Hamming code or Reed-Solomon (R-S) code.

Code II. inner code a convolutional code, outer code a block orthogonal code (MFSK).

Code III. inner code a convolutional code, outer code a R-S code.

Other methods of concatenation are possible. For example, two $k = 6$ by $v = 2$ convolutional codes can be concatenated to five a 9 by 4 code. Here k is the constraint length and $1/v$ is the rate of such a code. Each convolutional code can be decoded by using Viterbi's decoding scheme. Erickson [41] has shown, however, that the concatenation of Viterbi decoders does not appear to be useful in the

present context of the planetary program. He conjectured that the most appropriate outer code, in any concatenation scheme involving a Viterbi algorithm inner decoder, was a high-rate algebraic block code.

Consider first a generalized Hamming code as the outer code [38]. The code has n elements including k information (data) elements and m = n - k check elements. Each data element is a six-bit bi-orthogonal code word. The receiver performs both error detection and correction. The generalized Hamming code which has a Hamming distance of three is a specific case of R-S code. For the R-S code, the minimum distance d, between two code words is related to the number of check elements, m, by d = m + 1. The maximum number of correctable elements for each code word, t, is equal to m/2. The probability of the bit error after both error detection and correction is

$$P_c = \frac{P_A A_2 + P_B A_4}{A_2 + A_4} \tag{5.1}$$

where P_A = probability of bit error at the detector output, P_B = probability of bit error at the corrector output, and A_2 and A_4 are the normalized data quantities at the detector and the corrector outputs respectively [38].

Without restricting to the Hamming distance of 3, Forney [37] and Simpson [40] have considered the bi-orthogonal inner code and the R-S outer code. A typical concatenated coding system is shown in Fig. 13 where the R-S code can correct up to 2 errors. The main difference among the three reports [37], [38], [40], is in the decoding method. Forney considers both the maximum likelihood decoding and the generalized minimum distance decoding of the R-S code. Both Miller and Simpson use the algebraic decoding for the R-S code although their error probability expressions are inconsistent. The digit error given by Simpson is

$$P_D(e) \leq \sum_{i=t+1}^{n-t-1} \frac{(t+i)}{n} \binom{n}{i} P_e^i (1 - P_e)^{n-i} + \sum_{i=n-t}^{n} \binom{n}{i} P_e^i (1 - P_e)^{n-i} \tag{5.2}$$

where P_e is the probability of error of the bi-orthogonal code word. Available results are shown in Fig. 14 with the error probability plotted as a function of signal energy per bit to noise density ratio of the inner code. Curve 1 has a 2^8 - symbol R-S code and a bi-orthogonal code of rate 1/16 [37]. Curve 2 has a (18, 12) R-S outer code (12 information elements out of a total of 18 elements) and a 6 bit bi-orthogonal inner code [38]. Curve 3 has a (63, 49) R-S outer code and a 6 bit bi-orthogonal inner code [40]. Although the code lengths are not the same, it is clear that Curve 1 is better than Curve 2 which is better than Curve 3.

The block diagram of the concatenated system for Code II is shown in Fig. 15. Although it is possible to determine the upper bound of the error probability, the bound may be too loose to be useful. Some computer simulation results were reported by Richardson et.al. [44]. Let M be the bit-duration - IF filter bandwidth product. Figure 16 is a plot of the error probabilities for $v = 3$, $k = 6$ inner code and $v = 5$, $k = 8$ inner code with $M = 2$ and 10 along with the performance of the coherent systems without concatenation. The degradation in performance $M = 2$ to $M = 10$ is approximately 1.1 to 1.4 dB in E_b/N_o, the signal energy per bit to noise density ratio. It is noted that the performance improvement over the wideband noncoherent MFSK system [20] is very significant for both $M = 2$ and 10.

Code III was considered by Odenwalder [39]. A block diagram of the system is shown in Fig. 17. For any inner code of contraint length k bits, there exists a R-S outer code of block length $2^k - 1$ and with $2^k - d$ information bits. If P_e is the error probability of the convolutional inner code, then the word error probability with the R-S outer code is

$$P_w(e) = \sum_{t=\left\lceil \frac{d}{2} \right\rceil + 1}^{2^k-1} \binom{2^k-1}{t} P_e^t (1 - P_e)^{2^k-1-t} \tag{5.3}$$

where $d \geq 2t + 1$ and $\left\lceil \frac{d}{2} \right\rceil$ is the closest integer to d/2. Although analytical expression of error bound of Code III is available for very limited cases [46], the computer simulation result is more useful. The best computer simulation result of

(1/3, 8) convolutional inner code and 2^8 - symbol R-S outer code is shown in Fig. 18. Here v = 3, k = 8. Also plotted in the same figure are the error probabilities of a 5-bit bi-orthogonal code, an (1/2, 8) convolutional code with the Viterbi's maximum likelihood decoding (from Odenwalder [39], Chapter 5), and a concatenated code (31, 25, 5) with (31, 25) R-S outer code and 5 bit bi-orthogonal inner code. The improvement from bi-orthogonal only to bi-orthogonal/R-S code is added to the (1/2, 8) convolutional code to give an estimate of the error probability of a concatenated code with (1/2, 8) convolutional inner code and (31, 25) R-S code. The error probability of Code III is the best among all concatenated codes. The required interleave-buffer, however, essentially increases the word length, or reduces the effective signal-to-noise ratio.

Performance curves indicate that the concatenated codes greatly improve the peformance over the uncatenated codes. The decoding complexity increases from Code I to Code II to Code III while the performance improves in the reverse order. The decoding complexity depends manily on the inner code used. For the low available signal-to-noise ratio, Code III is definitely the best choice to keep the error rate also at a low level.

Chapter VI On the Spectrum of Split-Phase FSK

I. Introduction

It is now well known that the use of a split-phase baseband signal provides better DC response as compared with the use of a non return-to-zero (NRZ) baseband signal. The split-phase signal, however, requires a larger transmission bandwidth. The discrete frequency components that always exist in the spectrum of split-phase FSK facilitate acquisition and tracking of bit clock. Spectral analysis of the split-phase FSK has been reported by Hartmann [48], Shehadeh [49] and Chen [50]. Such analysis is needed to determine the bandwidth of the modultated signal and the magnitude of the discrete frequency components. In this chapter, we compare the expressions from Refs. [48] and [49] for the spectrum of split-phase FSK signals and determine the conditions under which the expressions coincide. One unique conclusion that can be made from all expressions is that the split-phase FSK has very significant discrete frequency components at the signalling frequencies, which are useful for bit synchronization.

II. The Spectrum of Split-Phase FSK

The paper by Hartmann [48] has presented a general and very useful expression for the spectrum of split-phase (Manchester coded) FSK with continuous phase. The main result of the paper is given by Eq. (14) which can be simplified to

$$\frac{1}{T} G(F) = \frac{1}{\pi^2} (\cos\pi D - \cos\pi F)^2 \frac{2D^2}{(F^2 - D^2)^2} + \frac{2}{\pi^2} \frac{(F\sin\pi F - D\sin\pi D)^2}{(F^2 - D^2)^2} \sum_n \delta(F - n) \quad (6.1)$$

where we have followed the notations of Ref. 48 and let T be the bit duration, $\omega_i = 2\pi f_i$, $i = 1,2$, be the two signalling frequencies, $2\Delta f = f_2 - f_1$, $f_2 \geq f_1$, $F = (f - f_c)T$, $f_c = \frac{1}{2}(f_1 + f_2)$, and $D = (\Delta f)T$ be the deviation ratio. The paper mentions the result by Shehadeh and Chiu [49] who assume that f_1 and f_2 are even integers multiplied by 1/T. Under this assumption, D is an integer ($D \neq 0$) and

Eq. (6.1) becomes

$$\frac{1}{T} G(F) = \frac{1}{\pi^2} ((-1)^D - \cos\pi F)^2 \frac{2D^2}{(F^2 - D^2)^2} + 0.5\,\delta(F - D) \tag{6.2}$$

where D is a positive integer.

The result in Ref. 49 mentioned above is the Eq. (66) which should be corrected to read,

$$\begin{aligned} S_{FSK-C}(\omega) = {} & \frac{A^2}{16}\delta(\omega - \omega_1) + \frac{A^2}{16}\delta(\omega + \omega_1) + \frac{A^2}{16}\delta(\omega - \omega_2) + \frac{A^2}{16}\delta(\omega + \omega_2) \\ & + \frac{A^2 t_o}{4}\left(\frac{\sin^2(\omega_1 - \omega)t_o/4}{(\omega - \omega_o)t_o/4}\right)^2 \cdot \frac{\sin^2\phi_1 + (\frac{\omega}{\omega_1})^2\cos^2\phi_1}{(1 + \omega/\omega_1)^2} \\ & + \frac{A^2 t_o}{4}\left(\frac{\sin^2(\omega_2 - \omega)t_o/4}{(\omega_2 - \omega)t_o/4}\right)^2 \cdot \frac{\sin^2\phi_2 + (\frac{\omega}{\omega_2})^2\cos^2\phi_2}{(1 + \frac{\omega}{\omega_2})^2} \\ & - \frac{A^2 t_o}{2} \frac{\sin^2(\omega_1 - \omega)t_o/4}{(\omega_1 - \omega)t_o/4} \cdot \frac{\sin^2(\omega_2 - \omega)t_o/4}{(\omega_2 - \omega)t_o/4} \\ & \times \frac{[\sin\phi_1\cos(\omega_1 - \omega)t_o/2 + \frac{\omega}{\omega_1}\cos\phi_1\sin(\omega_1 - \omega)t_o/2][\sin\phi_2\cos(\omega_2 - \omega)t_o + \frac{\omega}{\omega_2}\cos\phi_2\sin(\omega_2 - \omega)t_o/2]}{(1 + \frac{\omega}{\omega_1})(1 + \frac{\omega}{\omega_2})} \\ & - \frac{A^2 t_o}{2} \frac{\sin^2(\omega_1 - \omega)t_o/4}{(\omega_1 - \omega)t_o/4} \cdot \frac{\sin^2(\omega_2 - \omega)t_o/4}{(\omega_2 - \omega)t_o/4} \\ & \times \frac{[\sin\phi_1\sin(\omega_1 - \omega)t_o/2 - \frac{\omega}{\omega_1}\cos\phi_1\cos(\omega_1 - \omega)t_o/2][\sin\phi_2\sin(\omega_2 - \omega)t_o/2 - \frac{\omega}{\omega_2}\cos\phi_2\cos(\omega_2 - \omega)t_o/2]}{(1 + \frac{\omega}{\omega_1})(1 + \frac{\omega}{\omega_2})} \end{aligned} \tag{6.3}$$

where we have followed the notations of Ref. 49 with $t_o = T$. Since f_1 and f_2 are even integers multiplied by 1/T, the condition $\phi_1 = \phi_2$ is sufficient for the phase of the

signal to be continuous. Letting $\phi_1 = \phi_2 = \phi$ and averaging Eq. (6.3) over ϕ one gets after some simplification,

$$S_{FSK-C}(\omega) = \frac{A^2}{16}\delta(\omega - \omega_1) + \frac{A^2}{16}\delta(\omega + \omega_1) + \frac{A^2}{16}\delta(\omega - \omega_2) + \frac{A^2}{16}\delta(\omega + \omega_2)$$

$$+ \frac{A^2T}{8}\left(\frac{\sin^2(\omega_1-\omega)T/4}{(\omega_1-\omega)T/4}\right)^2 \frac{1 + (\frac{\omega}{\omega_1})^2}{(1 + \frac{\omega}{\omega_1})^2} + \frac{A^2T}{8}\left(\frac{\sin^2(\omega_2-\omega)T/4}{(\omega_2-\omega)T/4}\right)^2 \frac{1 + (\frac{\omega}{\omega_2})^2}{(1 + \frac{\omega}{\omega_2})^2}$$

$$- \frac{A^2T}{4} \cdot \frac{\sin^2(\omega_1-\omega)T/4}{(\omega_1-\omega)T/4} \cdot \frac{\sin^2(\omega_2-\omega)T/4}{(\omega_2-\omega)T/4} \cdot \cos(\omega_1 - \omega_2)T/2 \cdot \frac{1 + \frac{\omega}{\omega_1}\frac{\omega}{\omega_2}}{(1 + \frac{\omega}{\omega_1})(1 + \frac{\omega}{\omega_2})} \tag{6.4}$$

In the last term, $\cos(\omega_1 - \omega_2)T/2$ is always equal to one since f_1 and f_2 are even integers multiplied by $1/T$. Letting $A = 2$, folding the negative portion of the spectrum over to positive frequencies, and letting

$$D = \tfrac{1}{2}(f_2 - f_1)T, \quad F = (f - f_c)T, \quad f_c = \tfrac{1}{2}(f_1 + f_2)$$

one finds the normalized spectrum,

$$\frac{1}{T}G_{FSK-C}(F) = 0.5\,\delta(F - D)$$
$$+ \left(\frac{\sin^2\pi(F + D)/2}{\pi(F + D)/2}\right)^2 \cdot \frac{(f_cT - D)^2 + (f_cT + F)^2}{(2f_cT + F - D)^2}$$
$$+ \left(\frac{\sin^2\pi(F - D)/2}{\pi(F - D)/2}\right)^2 \cdot \frac{(f_cT + D)^2 + (f_cT + F)^2}{(2f_cT + F + D)^2}$$
$$- \frac{2\sin^2\pi(F + D)/2}{\pi(F + D)/2} \cdot \frac{\sin^2\pi(F - D)/2}{\pi(F - D)/2} \cdot \frac{(f_cT)^2 - D^2 + (f_cT + F)^2}{(2f_cT + F)^2 - D^2} \tag{6.5}$$

The discrete portions of the spectrum are identical in Eqs. (6.2) and (6.5). The continuous portion of the spectrum in Eq. (6.5) has been computed by H.P. Hartmann and is shown in Fig. 19. As we can see from the spectral plots, the two expressions

(Eqs. 6.2 and 6.5) agree for the case $f_cT >> D$. If this condition is not satisfied (dashed curves), the expression derived from Shehadeh and Chiu [49] takes into account the spectral foldover, while the expression from Hartmann [48] does not. In fact, it can be shown that the two expressions coincide for $f_cT >> D$, $f_cT >> F$, and D being a positive integer. If one let $f_cT >> D$ and $f_cT >> F$ in Eq. (6.5), one finds,

$$\frac{(f_cT - D)^2 + (f_cT + F)^2}{(2f_cT + F - D)^2} \simeq \frac{2(f_cT)^2}{4(f_cT)^2} = \frac{1}{2};$$

$$\frac{(f_cT + D)^2 + (f_cT + F)^2}{(2f_cT + F + D)^2} \simeq \frac{1}{2}; \quad \frac{(f_cT)^2 - D^2 + (f_cT + F)^2}{(2\,f_cT + F)^2 - D^2} \simeq \frac{1}{2}$$

and

$$\begin{aligned}\frac{1}{T} G_{FSK-C}(F) &= \frac{1}{2}\left[\frac{\sin^2\pi(F + D)/2}{\pi(F - D)/2} - \frac{\sin^2\pi(F - D)/2}{\pi(F - D)/2}\right]^2 \\ &= \frac{1}{2\pi^2}\left[\frac{1 - \cos\pi(F + D)}{(F + D)} - \frac{1 - \cos\pi(F - D)}{(F - D)}\right]^2 \\ &= \frac{1}{2\pi^2}\left[\frac{2D + (F - D)\cos\pi(F + D) + (F + D)\cos\pi(F - D)}{F^2 - D^2}\right]^2 \end{aligned} \tag{6.6}$$

in addition to δ term. If D is an integer, Eq. (6.6) reduces to Eq. (6.2) and thus verifies the computer results. If D is not an integer and if $f_cT >> D$, the two expressions do not coincide. For example, one may consider the special case F = D. Eq. (6.5) becomes

$$\frac{1}{T} G_{FSK-C}(F) = \left(\frac{\sin^2\pi F}{\pi F}\right)^2 \frac{2(f_cT)^2 + 2D^2}{(2f_cT)^2} \simeq \frac{1}{2}\left(\frac{\sin^2\pi F}{\pi F}\right)^2$$

In Eq. (6.1), by using L'Hospital's rule, the continuous spectrum becomes

$$\frac{2D^2}{\pi^2} \frac{(\cos\pi D - \cos\pi F)\sin\pi F}{F}\bigg|_{F=D} = 0$$

and the inconsistency is clear.

III. Concluding Remarks and Acknowledgement

We have shown that the two expressions of the spectrum of the split-phase FSK coincide if $f_c T >> D$, $f_C T >> F$ and D being a positive integer. Significant discrete spectral components occur at F = D, and D being a positive integer. It is assumed that the FSK signal has a continuous phase.

The author would like to thank H. Peter Hartmann of AG Brown, Boveri & Cie of Switzerland for the fruitful exchanges on this subject which lead to Ref. 9.

Chapter VII Computer Study of Phase-Locked Loop Behaviors at Low Data Rate

I. Introduction

The performance of command and telemetry systems, useful in deep-space communications, is frequently affected by the radio-frequency phase error which is introduced at the point of reception by means of the carrier tracking loop. In low data rate communications, this phase error may vary rapidly over the duration of the signaling interval. Causes of this type of behavior in planetary entry are turbulence, dispersion, attenuation and residual doppler. The phase variations cannot be tracked by a phase-locked loop of lower bandwidth, while the signal-to-noise ratio in this minimum loop bandwidth is too low.

When the ratio of the system data rate to carrier tracking loop bandwidth is less than one, the problem of power allocation between the carrier and the data has been considered by Hayes and Lindsey [51], Thomas [52], Sergo and Hayes [53]. For channels with time-varying phase, Heller [54] examined the performance of a sequential decoding system. An excellent treatment of the nonlinear analysis of the phase-locked loops is given by Viterbi [55] and Lindsey [56].

In this chapter the rapidly varying phase is characterized by a sinusoidal input phase, $k\sin(\omega_o t + \pi/6)$, which models a typical phase variation in communication over turbulent media. Nonlinear analysis of the phase-locked loop behaviors in the absence of noise has been performed by extensive computer study of the phase-plane trajectories [57], [58], [59], [60]. Readers interested in the detailed computer results should refer to Refs. 57-60. Only the problem formulation and the summary of the computer results are reported in the present chapter. Both the sinusoidal and the sawtooth phase detectors are considered. The sawtooth phase detector considerably improves the acquisition behavior of the phase-locked loop at low data rate [60].

II. The Loop Equation

Following the notations of Viterbi([55], Chapter 3), we consider first the differential equation of a second-order loop with perfect integrator.

$$\frac{d^2\phi}{dt^2} + AK\cos\phi\,\frac{d\phi}{dt} + aAK\sin\phi = \frac{d^2\theta_1}{dt^2} \tag{7.1}$$

where $\phi(t)$ is the phase error, AK is the loop gain, $\theta_1(t)$ is the phase of the input signal, and the transfer function of the loop filter is

$$F(s) = 1 + \frac{a}{s} \tag{7.2}$$

The loop can track the frequency ramp with zero steady state error. Now we consider the important case that $\theta_1(t)$ is varying several cycles over a bit interval of, say 1 second which is typical in low data rate communications. The variation is normally caused by the time-varying channel. Let

$$\theta_1(t) = k\sin(\omega_o t + \frac{\pi}{6}) \tag{7.3}$$

By normalizing the variables with

$$a' = \frac{a}{AK}\,,\quad \tau = AKt,\quad \phi' = \frac{d\phi}{d\tau}\,,\quad \phi'' = \frac{d^2\phi}{d\tau^2} \tag{7.4}$$

Eq. (7.1) becomes

$$\ddot{\phi} + \dot{\phi}\cos\phi + a'\sin\phi = -\frac{k\omega_o^2}{(AK)^2}\sin(\frac{\omega_o\tau}{AK} + \frac{\pi}{6}) \tag{7.5}$$

which in turn can be written in the state equation form as

$$\begin{aligned}\dot{x}_1 &= x_2\\ \dot{x}_2 &= -x_2\cos x_1 - a'\sin x_1 - \frac{k\omega_o^2}{(AK)^2}\sin(\frac{\omega_o\tau}{AK} + \frac{\pi}{6})\end{aligned} \tag{7.6}$$

where $x_1 = \phi(t)$. It is noted from Eq. (7.5) that the larger the loop gain, or the loop bandwidth, the smaller the frequency of the forcing function given by Eq. (7.3). The frequency f_o is reduced by a factor of AK, and the amplitude $k\omega_o^2$ is reduced by $(AK)^2$. In other words, the large loop gain reduces the effect of the time varying input phase $\phi_1(t)$.

For a third order loop with loop-filter transfer function

$$F(s) = 1 + \frac{a}{s} + \frac{b}{s^2} \tag{7.7}$$

the differential equation (Viterbi [55], p. 64) is

$$\frac{d^2\phi}{dt^2} + (AK\frac{d}{dt} + aAK)\sin\phi(t) + bAK\int_o^t \sin\phi(u)du = \frac{d^2\theta_1}{dt^2} \tag{7.8}$$

which, by using Eq. (7.4) and (7.3), can be reduced to

$$\ddot{\phi} + \dot{\phi}\cos\phi + a'\sin\phi + b'\int \sin\phi\, d\tau = -\frac{k\omega_o}{(AK)^2}\sin(\frac{\omega_o\tau}{AK} + \frac{\pi}{6}) \tag{7.9}$$

which in the state equation form becomes

$$\begin{aligned}\dot{x}_1 &= x_2\\ \dot{x}_2 &= -x_2\cos x_1 - a'\sin x_1 - b'\int \sin x_1\, d\tau - \frac{k\omega_o^2}{(AK)^2}\sin(\frac{\omega_o\tau}{AK} + \frac{\pi}{6})\end{aligned} \tag{7.10}$$

where

$$b' = \frac{b}{(AK)^2} \quad \text{and} \quad x_1 = \phi(t).$$

Phase-plane analysis of Eqs. (7.6) and (7.10) is performed by using the second-order Runge-Kutta method (see, e.g [59]). The computer results are reported in Refs. 57-59. A typical computer program is given as Appendix to this chapter.

If the sawtooth phase detector is used to replace the sinusoidal phase detector, the state equation becomes

$$\begin{aligned}\dot{x}_1 &= x_2\\ \dot{x}_2 &= -x_2 - a'\,\mathrm{saw}(x_1) - \frac{k\omega_o^2}{(AK)^2}\sin(\frac{\omega_o\tau}{AK} + \frac{\pi}{6})\end{aligned} \tag{7.11}$$

where

$$\mathrm{saw}(x) = x, \quad |x| \le \pi$$

and $\mathrm{saw}(x) = x \bmod 2\pi, \quad |x| > \pi$

Some comparison of the two phase detectors and the tanlock phase detector has been given by Long and Rutledge [61] and Uhran and Lindenlaub [62].

III. Summary of Computer Results

(1) Sinusoidal Phase Detector, Second-order Loop with Perfect Integrator

Consider first k = 0.001. The loop behavior depends on the ratio f_o/AK. It is noted that the steady state phase error cannot be reduced to zero because of the

continuous input phase variation. The condition for stability is the condition for the loop to settle with a stable "limit cycle." It is determined from the phase-plane study that $f_o/AK \leq 4$ is the condition for stability. The parameter values for the equality to hold are called threshold values. For specified (fixed) f_o, the threshold value of k depends on $a' = a/AK$. For $f_o = 1.1$ Hz, AK = 16, a = 8, $k_{th} = 1.661$. For fixed k, the threshold value for f_o is very sensitive to small parameter variation. For k = 10, AK = 16, a = 8. The threshold value can be determined from Figures 20, 21 and 22. The trajectory is still converging at $f_{oth} = 0.593$. It starts to diverge at $f_o = 0.5943$ and the loop is clearly unstable at $f_o = 0.5948$.

(2) Sinusoidal Phase Detector, Third-order Loop with Perfect Integrator

For k = 0.001, $f_o/AK \leq 1/4$ also appears to be the condition for stability. The increase of the parameter b' only causes the trajectory to drift more with larger steady state phase error [59]. A careful comparison [59] between the second-order and the third-order loops indicates that the third-order loop has no real advantage over the second-order loop at low data rate.

(3) Sawtooth Phase Detector, Second-order Loop with Perfect Integrator

For a = 8, AK = 16 and the specified values of f_o, the threshold values of k can be tabulated as follows:

f_o(Hz)	k_{th}(sawtooth)	k_{th}(sinewave)
1.1	8.98	1.661
1.0	10.60	3
0.8	16.215	5
0.5	40.5	10
0.25	163.0	50

where the estimated threshold values of k for the sinusoidal phase detector are also included.

For input signal phase with frequency ramp of slope R rad./sec^2, Viterbi ([55], Eq. 3.27) has shown that the condition for stability for the sinusoidal phase detector is $R' \leq a'$ where $R' = R/(AK)^2$. By using the sawtooth phase detector, the condition for stability is determined from the computer study as $R' \leq 3.017\ a'$ which is a considerable improvement over the sinewave phase detector.

Chapter VIII Coding/Modulation Selection and the Interplex System

I. Introduction

In this chapter we shall be concerned with the selection of coding/modulation techniques for the Pioneer-Venus main probe and small probe communication links [63]. We then discuss a very promising modulation system, namely interplex, a straight PCM/PSK approach which obtains a coherent demodulator reference for binary PSK when the carrier is completely suppressed.

II. Coding/Modulation Selection

The main probe communications link, like most space applications, is constrained by effective radiated power but not bandwidth. Hence coding to increase channel efficiency is desirable so long as the resulting complexity is manageable. Most coding techniques commonly used, however, are designed to improve efficiency of white Gaussian noise channels and are extremely sensitive to burst or fading effects which may be anticipated in the Pioneer-Venus missions. The heavily interleaved block-type codes designed for bursty channels are generally not very efficient. A solution is to concatenate two codes: an inner convolutional code and an outer Reed-Solomon (RS) with an interleaving buffering scheme as discussed in Chapter V. It is anticipated that when the channel is well behaved (i.e. not bursty), the E/N_o required will be 3 dB $\pm$ 1 dB with these codes. During periods of deep fading most errors will be corrected provided that the fading characteristics have been reasonably well predicted and the channel is below threshold no more than 30% of the time [64]. Certain convolutional codes, namely the diffuse threshold-decoded convolutional and Gallager's adaptive error correcting scheme are capable of correcting random errors and extended error bursts and are thus suited to channels with memory. To design such codes effectively, it is necessary to understand the fading spectrum rather well. Presently the precise fading characteristics are not available (see Chapter IV). We have to make use of the best available information in code design.

From the nature of the convolutional coding systems and from test results, it is found [65] that the Gallager code is more suitable to channels where bursts are dense and intervals between bursts are clean, and the diffuse code is optimum for channels where bursts are more gradual and background error rate is not negligible. The adaptive Gallager code [66]which employs convolutional coding to combat random errors and a form of time diversity to combat burst errors appears to meet the needs for the communication situation under consideration. The reasons are:

(1) It offers the simplicity attendant to using Viterbi decoding algorithms when the channel is not experiencing severe fading.

(2) The bursty channel actually exists for a small percentage of the overall mission duration. The code is suitable for both bursty and additive Gaussian noise channels.

(3) Test results indicate that at a burst-correction capability of about 6 seconds, the code is error-free 90 percent of the time which is much better than the use of simple diversity system. This capability is adequate for the Venus atmospheric channel as the average duration for each deep fade is less than 6 seconds. Errors in the guard space, however, must be corrected as much as possible.

Modulation choices are not independent of the coding choice. Two types of modulation have been considered for use with heavily coded systems. These are coherent PCM/PSK/PM and noncoherent MFSK. Generally the coherent system is more efficient except at very low data rates in that case the noncoherent system is better. It appears that the baseline modulation/coding scheme for the large probe should be based on coherent PCM/PSK/PM modulation with convolutional inner and RS outer codes.

Small probe communication geometry is similar to that of the large probe, particularly during the terminal descent phases; that the communications environment will be essentially the same. In particular, the possibility of deep signal fades due to atmospheric turbulence will be present. Consequently, the coding approach

suggested for the large probes, a convolutional inner code concatenated with a RS interleaved outer code, is also appropriate for the small probe. With regard to modulation, however, the low data rate for the small probe results in a poorer ratio of the required carrier power to data channel power, in a PSK/PM system, than was the case in the large probe. In this case the noncoherent MFSK system would be a better choice.

III. The Interplex System

It is well known that maximum efficiency of a coherent single-channel PCM/PSK/PM system is achieved by completely suppressing the RF carrier, and that a coherent local carrier reference required to demodulate can be established by means of a Costas loop [67], a squaring loop [55] or another type of decision-directed tracking loop. However, in the existing two-channel system, it is theoretically not possible to completely suppress the RF carrier without simultaneously eliminating one of the channels. Recently a new two-channel modulation scheme called Interplex [68] has been suggested where the intermodulation loss and the RF carrier power can be eliminated without compromising any of the advantages of the existing system. Not only is the Interplex system more efficient than the existing system, when some unsupppressed RF power is transmitted, but it permits 100% of the transmitted power to be allocated to data-bearing sidebands while preserving two-channel PCM/PSK/PM operation at all ratios of channel powers. In this mode, the RF carrier is completely suppressed; therefore, it is necessary to develop a method for maintaining frequency and phase sync at the receiver by methods other than the standard phase-locked loop.

It can be shown that although Costas or squaring loops can be used, their performance deteriorates rapidly as the ratio of the channel powers (or data rates) $\alpha = P_2/P_1$ increases until no tracking is feasible when $\alpha = 1$. Timor and Burman [69]

developed methods for tracking the phase of a suppressed carrier for the two-channel Interplex system. The resulting RF power will be independent of α. They also considered the performance of the system in the presence of noise. Further comparison between the conventional and the Interplex system is available in Ref. 70.

The Interplex system offers a good possibility for maintaining coherent operations in both large probe and small probe communication links. Performance of the system in the presence of deep fades remains to be studied.

Chapter IX Conclusion and Further Work

I. Conclusion

In his efforts to understand more about distant planets via unmanned space missions, man has benefited far more than the knowledge he gained about such planets. In the communication system design, for instance, there have been numerous problems which were never experienced before in commercial and military communication applications. The research and development efforts in deep space communications have added an important dimension to the field of communications. For the first time there is considerable study in designing communication receivers operating in the presence of large frequency uncertainty [71]. The possibility of deep fades due to the Venus atmosphere has prompted careful study of the Venus channel. A need for high communication efficiency leads to intensive efforts of designing better codes such as the concatenated code, and decoding algorithms. The availability of new digital processing techniques has improved the software receiver design. These have been the topics in the present report.

It is reasonable to conclude that, although there are still many problems to be studied, we now have a much better understanding of the low data rate digital space communications. Continued efforts in these studies will assure the success of the forthcoming untried deep space missions. And many of the results we obtain from these studies will also be very useful for solving the communication problems on earth.

II. Recommendations for Further Work

In Chapter II, the software or hardware implementation of the proposed all-digital system is recommended.

In Chapter III, re-evaluation of the system performance is recommended when more precise fading characteristics become available.

In Chapter IV, precise fading characteristics remain to be examined.

In Chapter V, the best available performance from using the concatenated code (Code III) must be evaluated theoretically.

In Chapter VI, further study is needed on the power spectral density of the angle modulated signal with split-phase baseband format.

In Chapter VII, theoretical analysis of the phase-locked loop behaviors with rapidly varying phase error is much needed. Further computer study on the third-order loop is also recommended.

In Chapter VII, the modulation selection for small probe communication link needs further study in view of the available Interplex system.

REFERENCES

1. R.M. Goldstein, "Low Data Rate Communication: Block-Coded Frequency Shift Keying", JPL Space Programs Summary, 37-35, Vol. II, pp. 30-36, 1969.

2. M.J. Ferguson, "Communication at Low Data Rates - Spectral Analysis Receivers," IEEE Trans. on Communication Technology, Vol. COM-16, No. 5, pp. 657-668, October, 1968.

3. C. H. Chen and M. Fan, "An All Digital Low Data Rate Communication System", International Telemetering Conference Proceedings, Washington, D. C., Oct. 9-11, 1973. Also appeared as NASA Report N73-22077, CR-130234, available from NTIS.

4. H.D. Chadwick and J. C. Springett, "The Design of a Low Data Rate MFSK Communication System," IEEE Trans. on Communication Technology, vol. COM-18, No. 6, pp. 740-750, December 1970.

5. H. D. Chadwick, "The Error Probability of a Wide-band FSK Receiver in the Presence of Multipath Fading", IEEE Trans. on Communication Technology, Vol. COM-19, No. 5, pp. 699-707, October 1971.

6. C.H. Chen, "Effects of Multipath Fading on Low Data-Rate Space Communications", International Telemetering Conference Proceedings, Los Angeles, Oct. 10-12, 1972.

7. D.A. DeWolf, "Atmospheric Turbulence on Venus: Venera 4, 5, 6, and Mariner 5 Estimates", Journal of Geophysical Research, Vol. 76, No. 13, pp. 3154-3158, May 1971.

8. I. Bar-David and S. Butman, "Performance of Coded, Noncoherent, Hard-Decision MFSK Systems," JPL Technical Report 32-1526, Vol. XIII, pp. 82-91, Feb. 15, 1973.

9. C.H. Chen and H.P. Hartmann, "Comments on the Spectrum of Manchester Coded FSK", IEEE Trans. on Communications, Feb. 1974.

10. R. Winkelstein, "Spectral Estimate Variance Reduction by Averaging FFT Spectra of Overlapped Time Series Data", The Deep Space Network, JPL Technical Report 32-1526, Vol. VII, pp. 74-80, February 15, 1972.

11. H.D. Chadwick, "Frequency Tracking in an MFSK Receiver", JPL Space Programs Summary, 37-57, Vol III, pp. 47-53.

12. M.K. Simon, "Progress Report on MFSK Tracking", unpublished, October 1973.

13. A.V. Oppenheim and C.J. Weinstein, "Effects of Finite Register Length in Digital Filtering and the Fast Fourier Transform", Proc. of the IEEE, Vol. 60, No. 8, pp. 957-976, August 1972.

14. T. Kaneko and B. Liu, "Accumulation of Round-off Error in Fast Fourier Transforms", Journal of the Association for Computing Machinery, Vol. 17, No. 4, pp. 637-654, October 1970.

15. A. Kliore, et al, "Structure of the Atmosphere of Venus Derived from Mariner V S-band Measurements," in Space Research IX, North Holland Publishers Co., Amsterdam, pp. 712-729, 1969.

16. G. Fjeldbo, A. J. Kliore and V. R. Eshelman, "The Neutral Atmosphere of Venus as Studied with the Mariner V Radio Occulation Experiments," The Astronomical Journal, Vol. 76, No. 2, pp. 123-127, March 1971.

17. A. B. Glenn, "Fading from Irregular Surfaces for Line-of-Sight Communications," IEEE Trans. on Aerospace and Electronic Systems, Vol. AES-4, No. 2, pp. 149-163, March 1968.

18. L. Schuchman, "Wide-band Detection of FSK Transmission in a Three-Component-Two-Path Channel," IEEE Trans. on Communication Technology, Vol. COM-18, No. 4, pp. 319-332, August 1970.

19. P. Beckman and A. Spizzichino, "The Scattering of Electromagnetic Waves from Rought Surfaces", MacMillan, New York, 1963.

20. C.H. Chen, "Error Probability of Wideband Noncoherent Multiple Frequency Shift Keyed Scheme," Proc. of the IEEE, Vol. 55, No. 12, December 1967.

21. W. C. Lindsey, "Coded Noncoherent Communications", IEEE Trans. on Space Electronics and Telemetry, Vol. SET-11, pp. 6-13, March 19 5.

22. D.A. DeWolf and J.W. Davenport, "Investigation of Line-of-Sight Propagation in Dense Atmosphere: Part I", Final Report, May 1969-May 1970, Contract No. NAS 2-5310 for NASA ARC.

23. J.W. Davenport and D.A. DeWolf, "Investigation of Line-of-Sight Propagation in Dense Atmosphere: Part II," Section V, Final Report, July 1971, Contract No. NAS 2-5310 for NASA ARC.

24. M.A. Kolosov, O.I. Yakovlev and A.I. Yefimov, "Propagation of Radiowaves in the Atmosphere, of Venus from the Data of 'Venus 4', 'Venus 5' and 'Venus 6'", Radio Engineering and Electronic Physics, Vol. 15, No. 12, pp. 2183-2188, 1970.

25. O.I. Yakovlev, A.I. Efimov, and T.S. Timofeeva, "Venera-7 Spaceprobe Data on Propagation of Radio Waves through the Venusian Atmosphere and through the Interplanetary Plasma," Cosmic Research, translated from Russian, 1971.

26. J.W. Strohbehn, "The Effect of Turbulence in the Venus Atmosphere on Radio Propagation," August 14, 1973, to be published. This paper is an extension of numerous unpublished works which Dr. Strohbehn performed for AVCO Systems Division, Wilmington, Mass. in 1972.

27. Y.N. Aleksandrov, O.N. Rzhiga, and A.M. Shakhovskoi, "Digital computer analysis of radio signals transmitted by the Soviet Venera-7 interplanetary station landing on the surface of Venus", Cosmic Research, translated from Russian, 1971.

28. V.V. Kerzhanovich, "Wind velocity and turbulence in the Venusian atmosphere, as obtained from the data of doppler meaasurements of the velocity of the automatic interplanetary stations Venera-4, Venera-5, and Venera-6", Cosmic Research, translated from Russian, 1972.

29. M.A. Kolosov, O.I. Yakolev, and A.I. Yefimov, "Study of the propagation of decimeter radiowaves in the atmosphere of Venus with the aid of AIS Venera-4", Doklady, A.N. SSR, Geofixika, Vol. 182, 1968.

30. A.S. Gurvich, "An estimate of the small-scale turbulence parameters in the Venus atmosphere by radio signal fluctuations of Venera-4 and Mariner-5", Diklady, Akad, Nauk, SSR, Fizika Atmosfery i Okeana, Vol. 5, 1969.

31. V.S. Avduevsky, M. Ya. Marov, M.K. Rozhdestvensky, N.F. Brodin, and V.V. Kerzhanovich, "Landing of the automatic station Venera-7 on the Venus surface and preliminary results of investigations of the Venus atmosphere", Cosmic research, translated from Russian, 1971.

32. Pioneer Venus, Report of a Study by the Science Steering Group," NASA Ames Research Center, June 1972.

33. V.I. Tatarski, "Wave Propagation in a Turbulent Medium", translated from the Russian by R.A. Silverman, McGraw-Hill Book Co., 1961.

34. K.A. Norton, et al, "The Probability Distribution of the Amplitude of a Constant Vector plus a Rayleigh Distributed Vector," Proceedings of the IRE, pp. 1354-1361, October 1955.

35. J.W. Strohbehn, private communications, August and September 1973.

36. C.H. Chen, "Atmospheric Effects on R.F. Propagation due to Turbulence in the Venus Atmosphere", Proceedings of the National Telecommunications Conference, Atlanta, Ga., November 1973.

37. G. D. Forney, Jr. "Concentrated Codes", M.I.T. Press, Cambridge, Mass. 1966.

38. B. Dorsch and W. H. Miller. "Error Control Using a Concatenated Code," NASA TN D-5775, Goddard Space Flight Center, Greenbelt, Md. June, 1970.

39. J. P. Odenwalder. "Optimal Decoding of Convolutional Codes," Ph.D. Thesis, University of California, Los Anglees, Chapter 6, 1970.

40. R. S. Simpson and J. B. Cain. "A Study of Major Coding Techniques for Digital Communication,"Final Report, NASA-CR-102447, N70-19873, 1970.

41. D. Erickson. "Concatenation of Short Constraint Length Convolutional Codes," JPL Technical Report 32-1526, Vol. 1, pp. 46-51, 1970.

42. B. Dorch. "Information Content of Error Correcting Codes," IEEE International Symposium on Information Theory, Ellenville, N.Y. January 1969.

43. J.E. Savage. "A Note on the Performance of Concatenated Codes," IEEE Trans. on Information Theory, Vol. IT-16, No. 4, July 1970.

44. R. J. Richardson, C. C. Korgel and R. B. Blizard, "Coding for Low Data Rate Noncoherent Channels", National Telemetering Conference Record, pp.233-239, April 1971.

45. A. K. Choudhury, "Performance of Convolution Coding Concatenated with M-ary Non-coherent Frequency Shift Keyed (MFSK) Communication Link in Planetary Exploration", NASA/GFSC Technical Report, Dec. 1971.

46. J. W. Modestino, unpublished report on the error probability of M-ary convolutional codes, 1972.

47. C. H. Chen, "Concatenated Coding for Low Data Rate Space Communications", International Telemetering Conference Proceedings, Los Angeles, Cal., October 1972.

48. H. P. Hartmann, "Spectrum of Manchester Coded FSK", IEEE Trans on Communications, pp. 1001-1004, October 1972.

49. N. M. Shehadeh and R. F. Chiu, "Transmission Characteristics of Split-phase PCM Codes", NASA Final Report, Part I, Contract NAS 9-9270, March 1970.

50. C. H. Chen, "Split-phase PCM/FM and PCM/PM Power Spectra", Journal of Electrical Engineering, National Taiwan University, Taipei, Taiwan, January 1970.

51. J. F. Hayes and W. C. Lindsey, "Power Allocation - Rapidly Varying Phase Error", IEEE Trans. on Communication Technology, pp. 323-326, April 1969.

52. C. M. Thomas, "Carrier Reference Power Allocation for PSK at Low Data Rates", International Communications Conference, June 1970.

53. J. R. Sergo, Jr. and F. J. Hayes, "Power Allocation in a Two Way Coherent Communication Systems", UMR-M. J. Kelly Communications Conference, paper no. 22-2-1, Rolla, Mo., October 1970.

54. J. A. Heller, "Sequential Decoding for Channels with Time-varying Phase", Ph.D. thesis, M.I.T., Cambridge, Mass. September 1967.

55. A. J. Viterbi, "Principles of Coherent Communication", McGraw-Hill Book Co., 1966.

56. W. C. Lindsey, "Synchronization Systems in Communication and Control", Prentice-Hall, Inc., 1972.

57. C. H. Chen, "Phase-Plane Analysis of Phase-locked loops with Rapidly Varying Phase", TR EE-73-4, SMU, No. Dartmouth, Mass., July 1973.

58. M. Fan, "Computer Study of Phase-locked Loop Behaviors with Rapidly Varying Phase Error," TR EE-73-5, SMU, No. Dartmouth, Mass., September 1973.

59. C. H. Chen and M. Fan, "Nonlinear Analysis of Phase-locked Loops with Rap dly Varying Phase", TR EE-73-6, SMU, No. Dartmouth, Mass., October 1973.

60. M. Fan, "Comparison of Sinuoidal and Sawtooth Phase Detectors for Phase-locked Loops with Rapidly Varying Phase," TR EE-73-8, November 1973.

61. L. L. Long and R. B. Rutledge, "A Digital Computer Simulation for Comparative Phase-Locked Loop Analysis", Proceedings of National Electronics Conference, 1965.

62. J. J. Uhran, Jr. and J. C. Lindenlaub, "Experimental Results for Phase-locked Loop Systems Having a modified nth-order Taplock Phase Detector", IEEE Trans. on Communication Technology, vol. COM-16, no. 6, pp. 787-795, Dec. 1968.

63. "A Proposal for a Venus Pioneer Systems Design study", vol. 1 - Technical, prepared by AVCO Systems Division, for NASA Ames Research Center, May 1972.

64. G. D. Forney, Jr. Burst-Corecting Codes for the Classic Bursty Channel", IEEE Trans on Communication Technology, vol. COM-19, no. 5, pp. 772-781, October 1971.

65. A. Kohlenberg and G. D. Forney, Jr., "Convolutional Coding for Channels with Memory", IEEE no. 5, pp. 618-626, September 1968.

66. D.D. Sullivan, "A Generalization of Gallager's Adaptive Error Control Scheme," IEEE Trans. on Information Theory, vol. IT-17, pp. 727-735, November 1971.

67. J. P. Costas, "Synchronous Communication", Proc. IRE, vol. 44, no. 12, pp. 1713-1718, December 1956.

68. JPL Space Program Summary, 37-62, vol. III, pp. 57-60.

69. U. Timor and S. Butman, "Space Station Unified Communication: Suppressed - Carrier Two-channel Interplex Modulation System", JPL Space Program Summary 37-64, vol. III, pp. 27-31.

70. S. Butman and U. Timor, "Interplex - An Efficient Multichannel PSK/PM Telemetry System", IEEE Trans. on Communications, vol. COM-20, no. 3, June 1973.

71. C. H. Chen, "Evaluation of Communication Systems Operating with Large Frequency Uncertainty", TR EE-73-7, SMU, No. Dartmouth, Mass., October 1973.

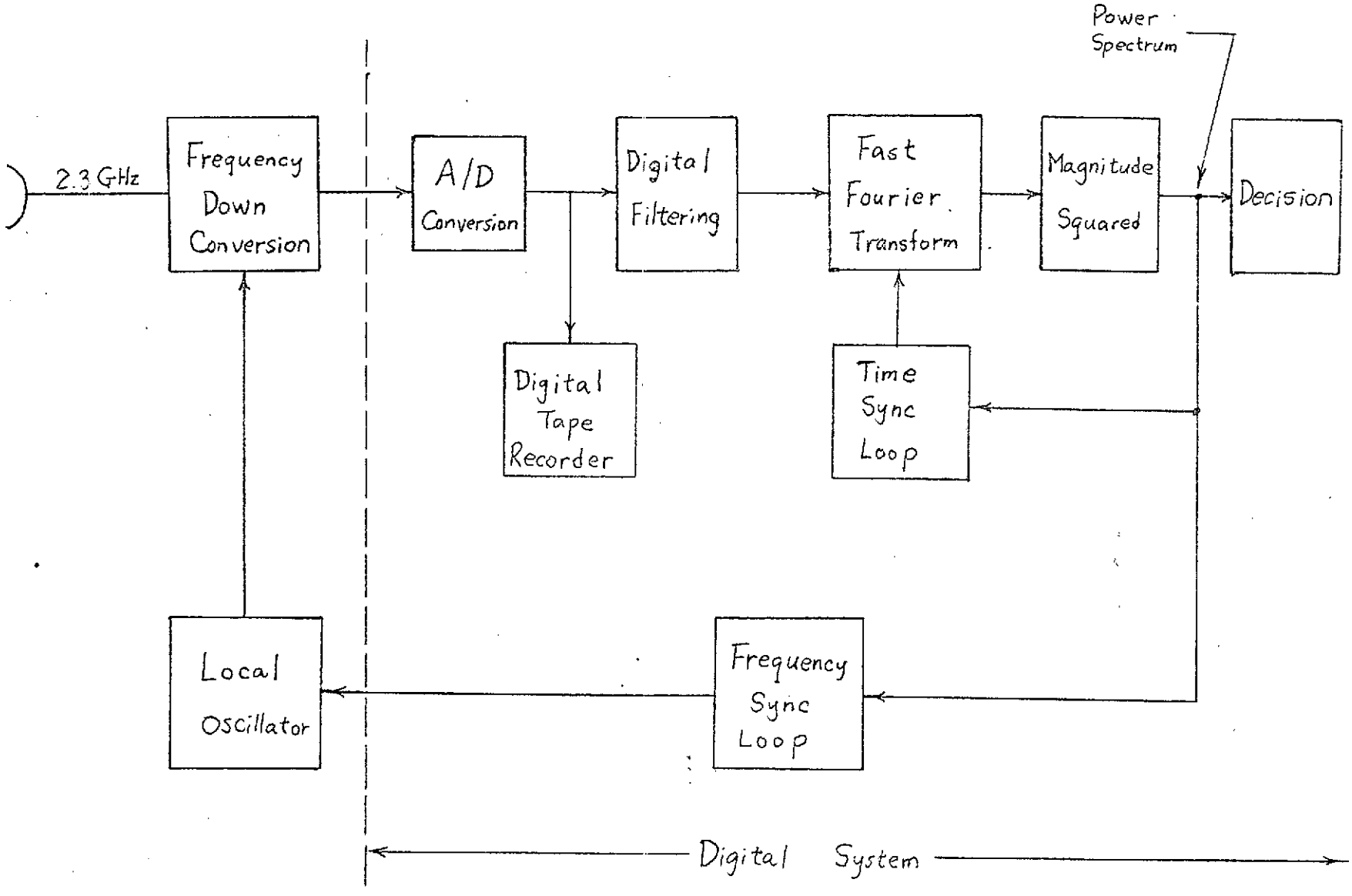

Fig. 1 Proposed Low Data Rate Communication System

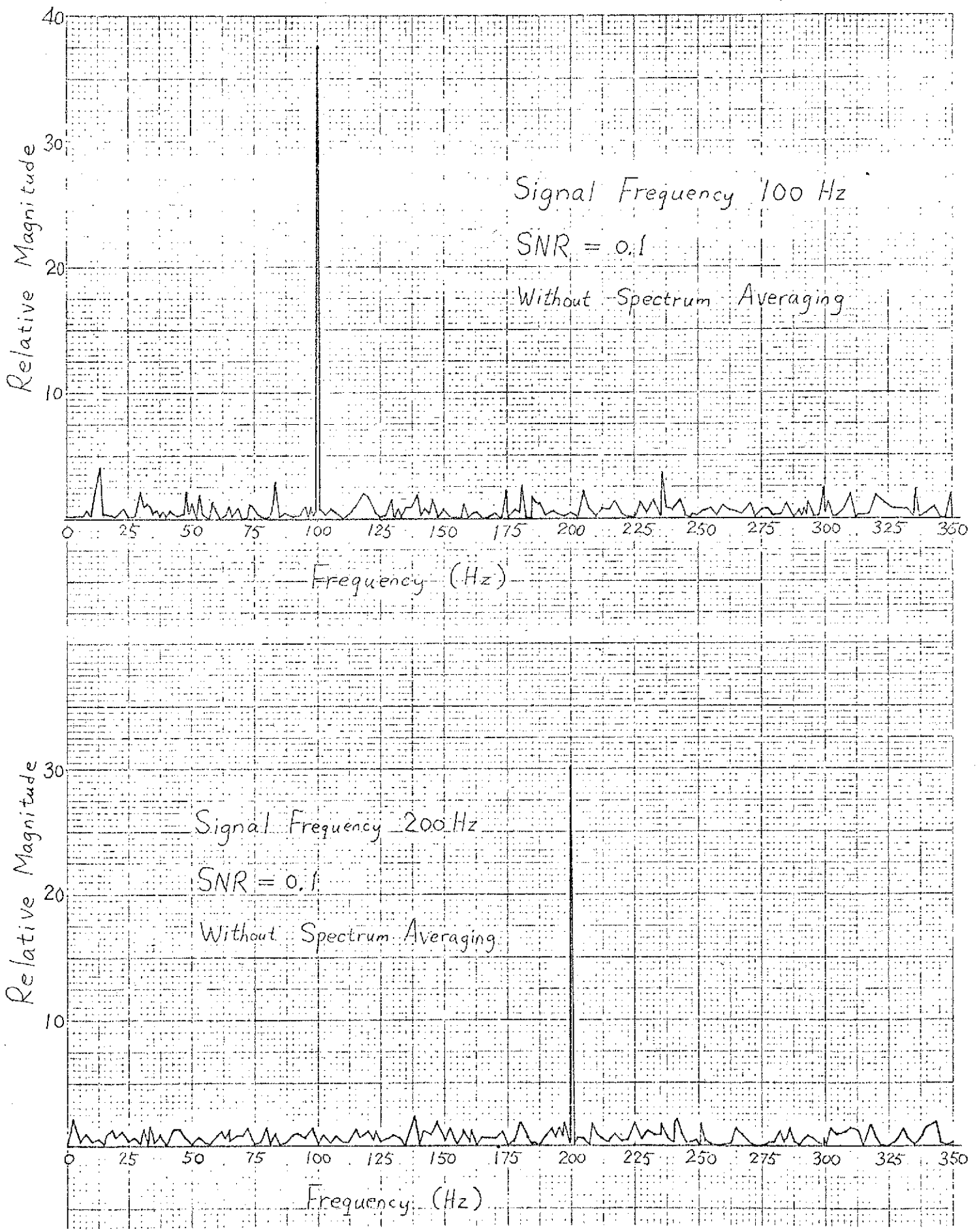

Fig. 2 Power Spectrum of a FSK Signal plus Noise

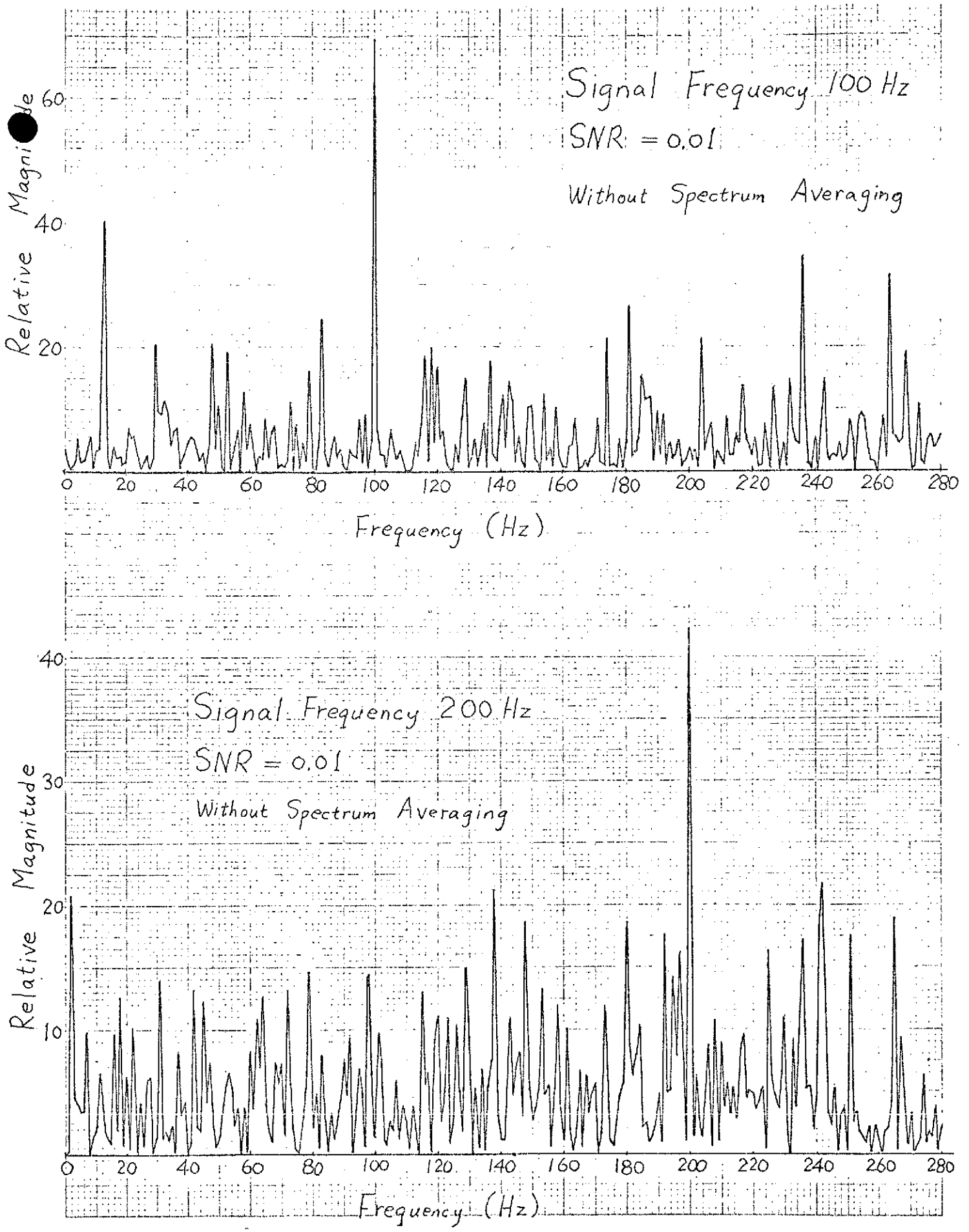

Fig. 3 Power Spectrum of a FSK Signal plus Noise

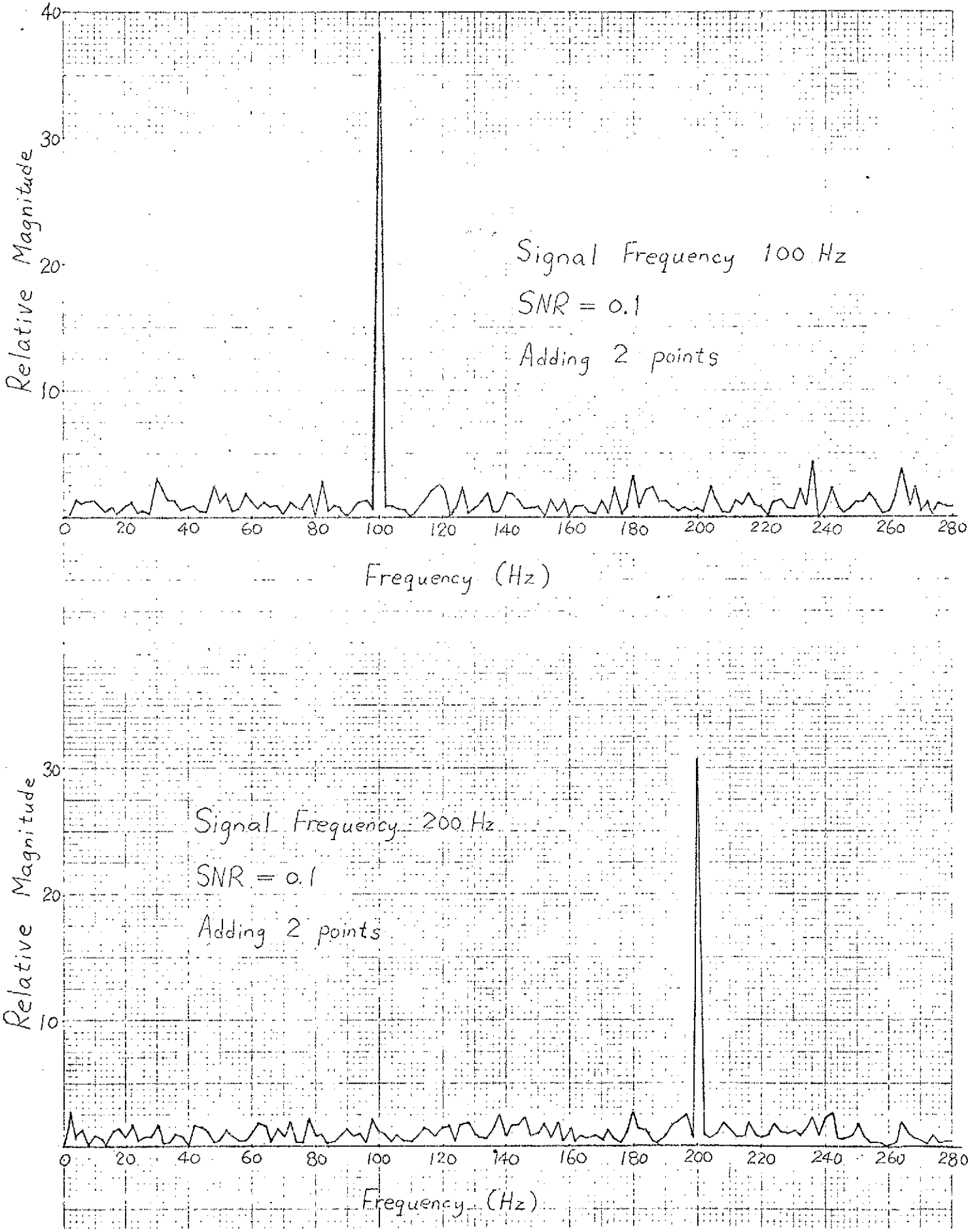

Fig. 4a Power Spectrum of a FSK Signal plus Noise

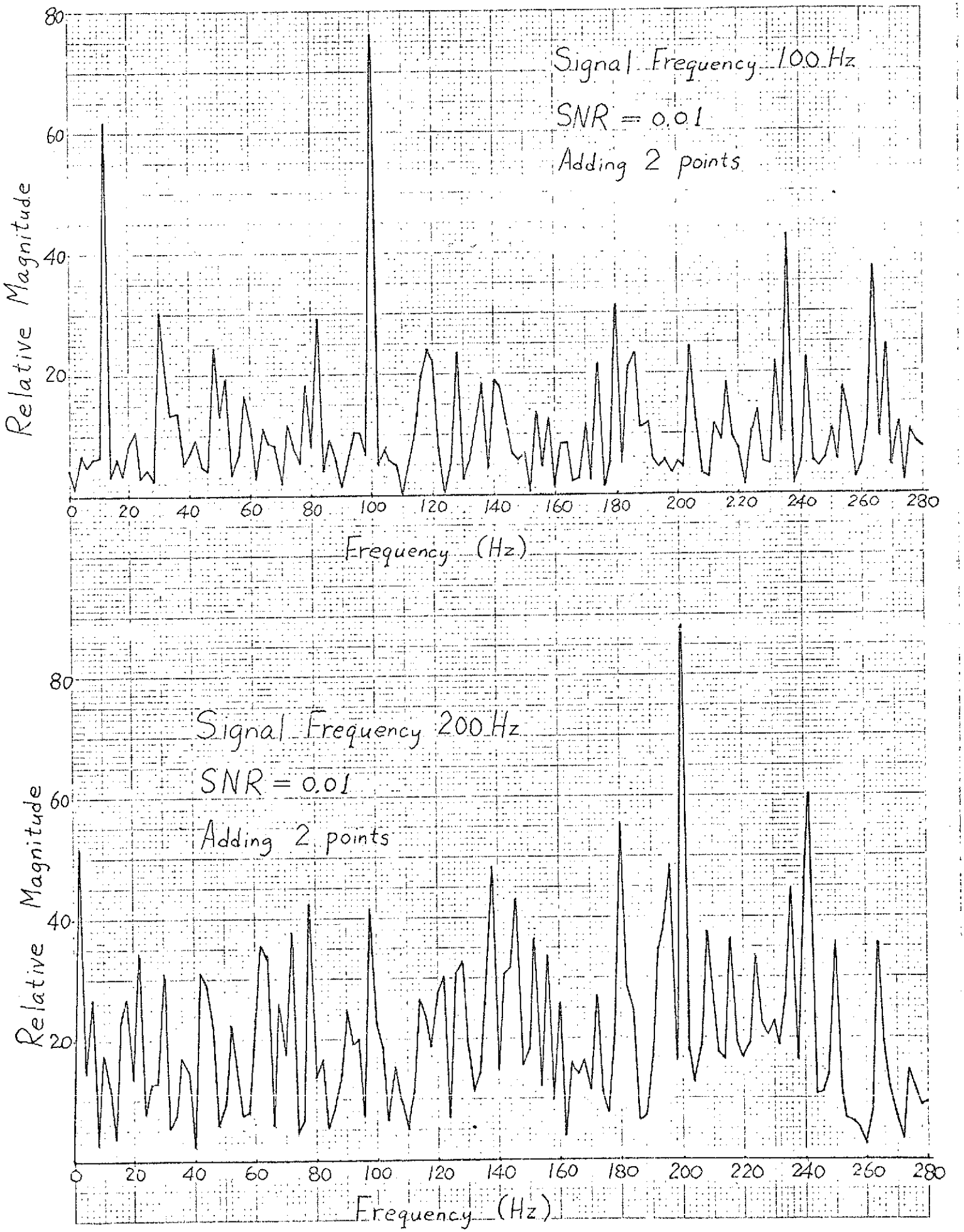

Fig. 4b Power Spectrum of a FSK Signal plus Noise

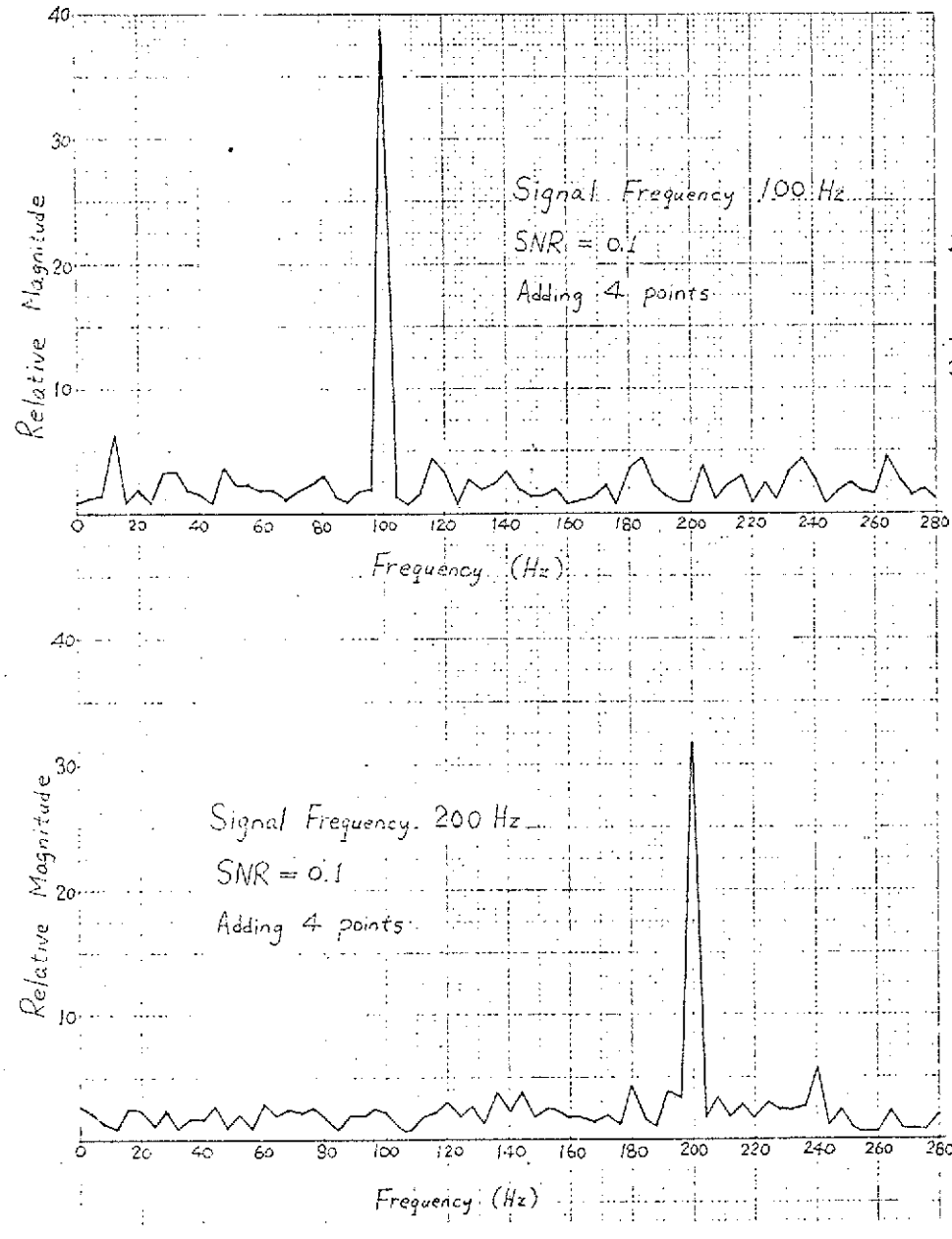

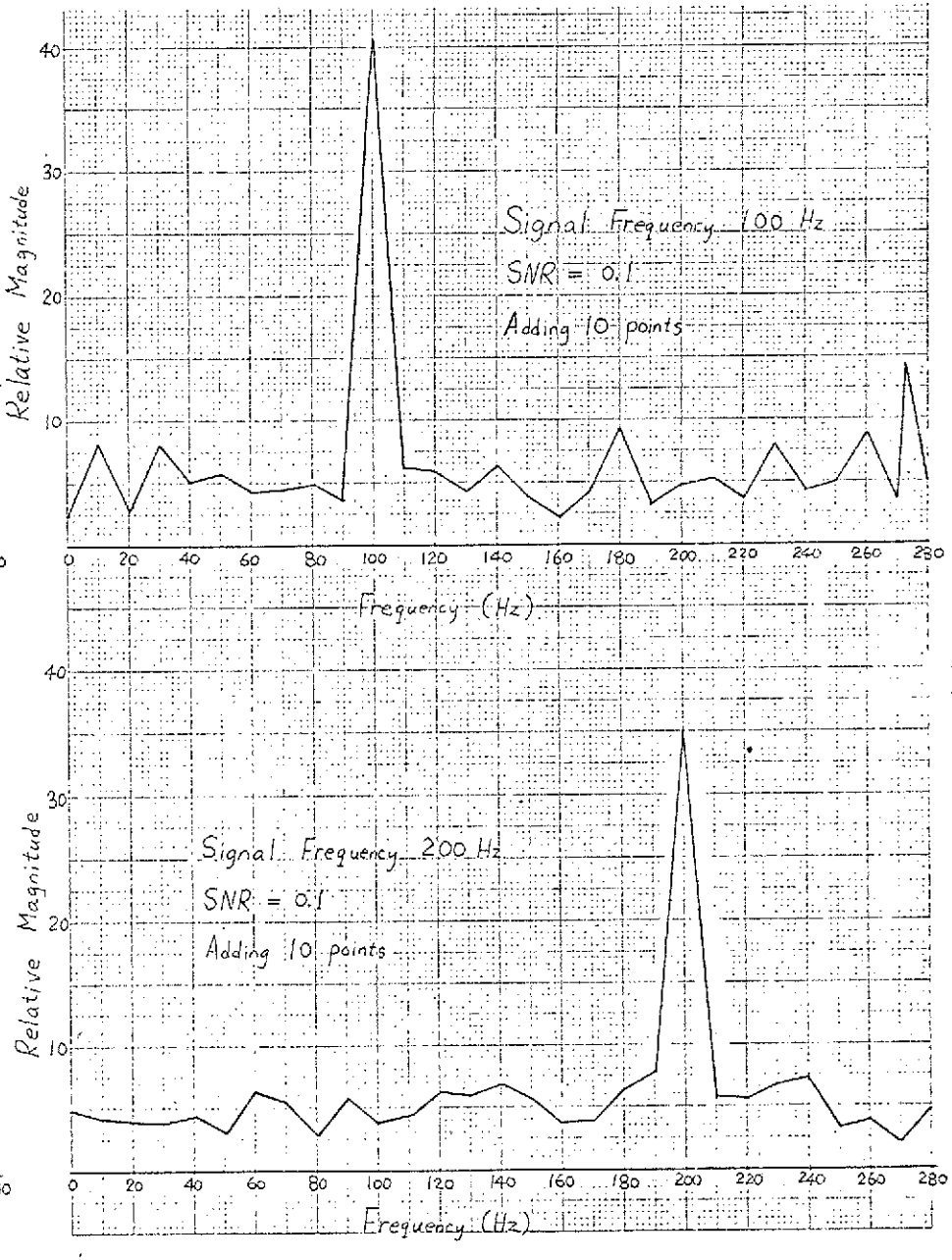

Fig. 5 Power Spectrum of a FSK Signal plus Noise

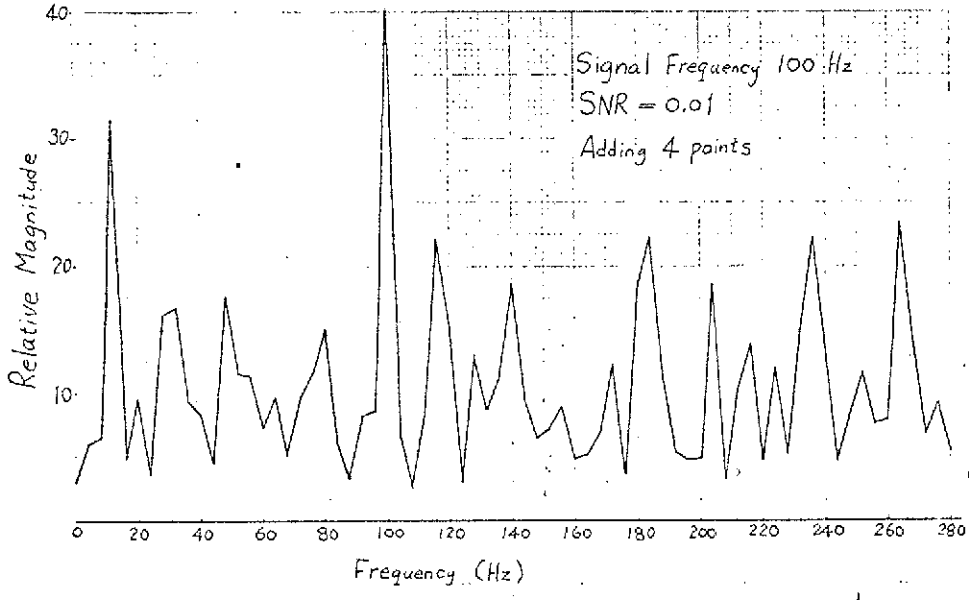

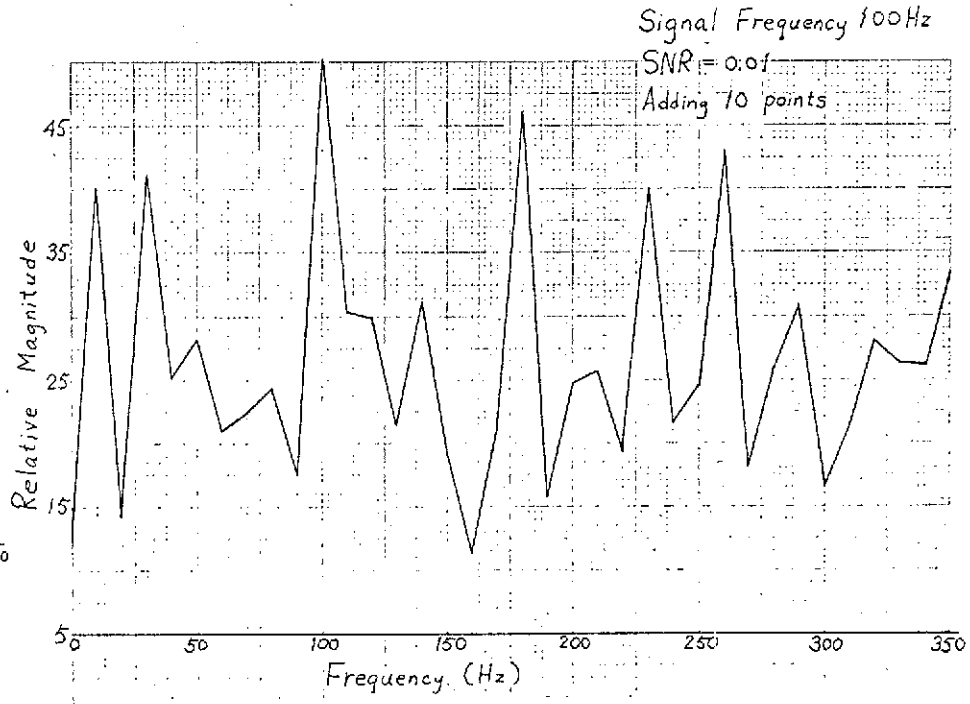

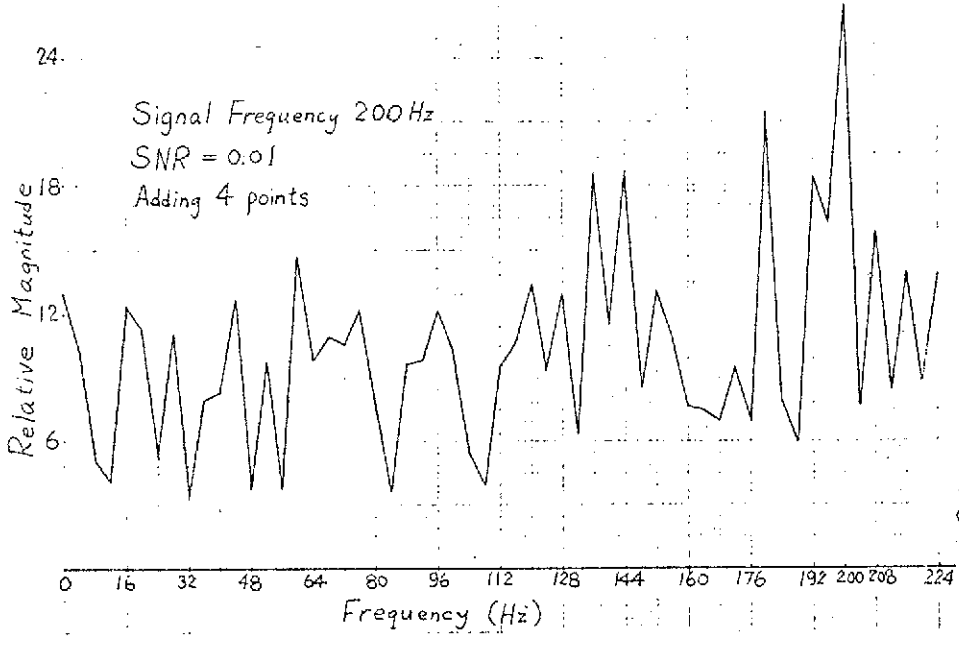

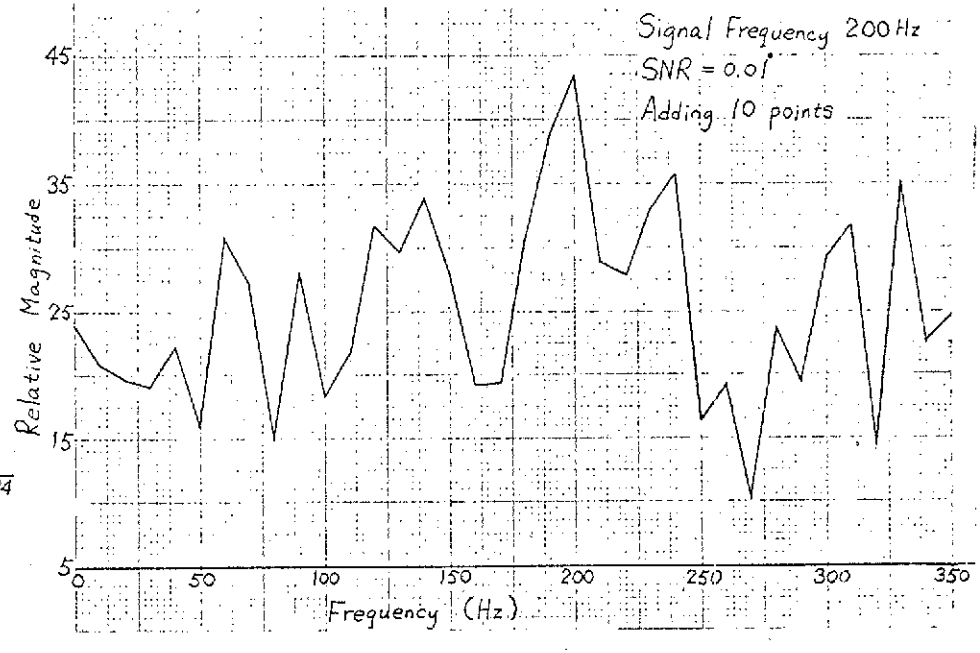

Figure 6

Power Spectrum of FSK Signal plus Noise

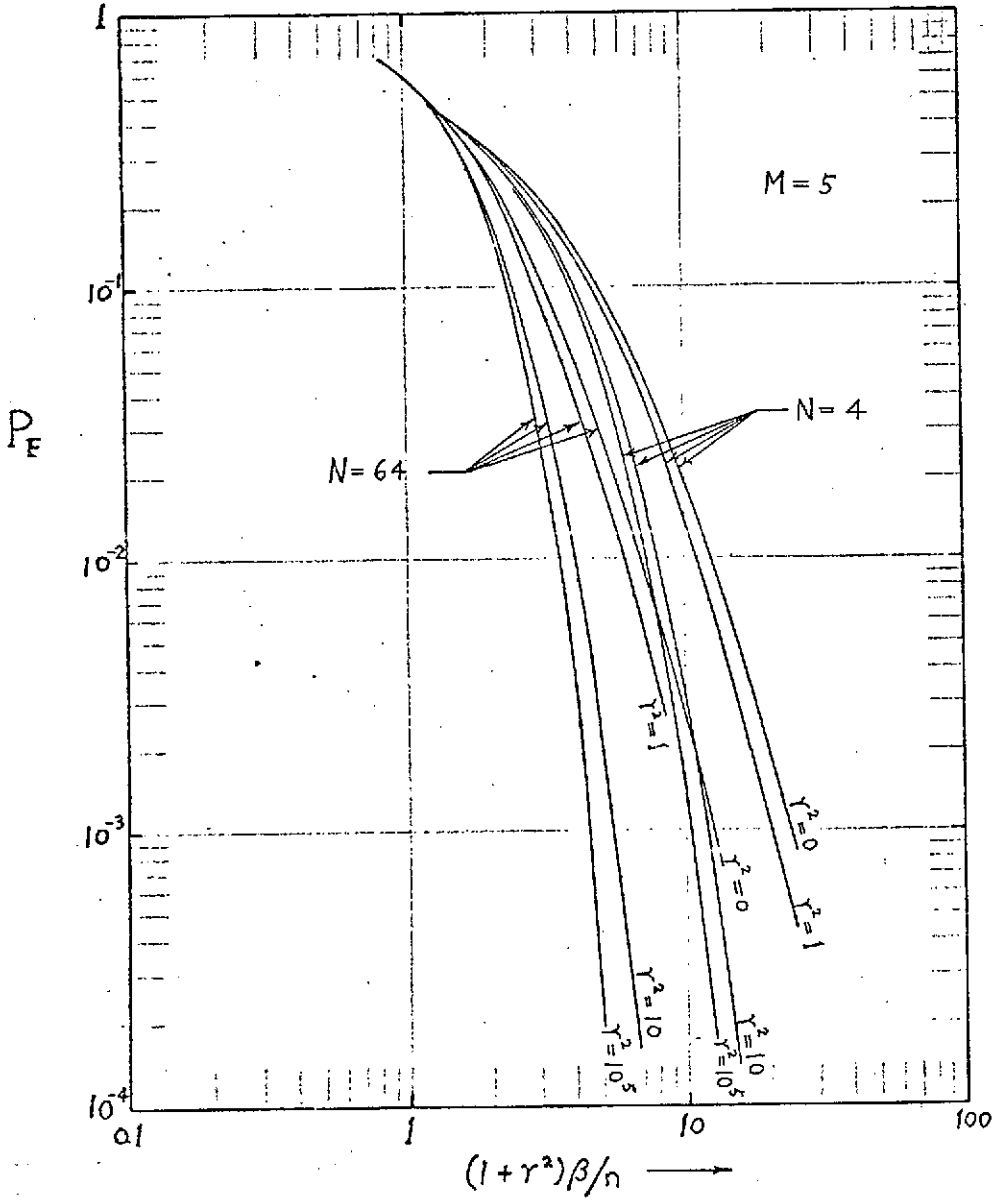

Fig. 7 Word Error Probability of Wideband Noncoherent MFSK Receiver with Multipath Fading (M = 5)

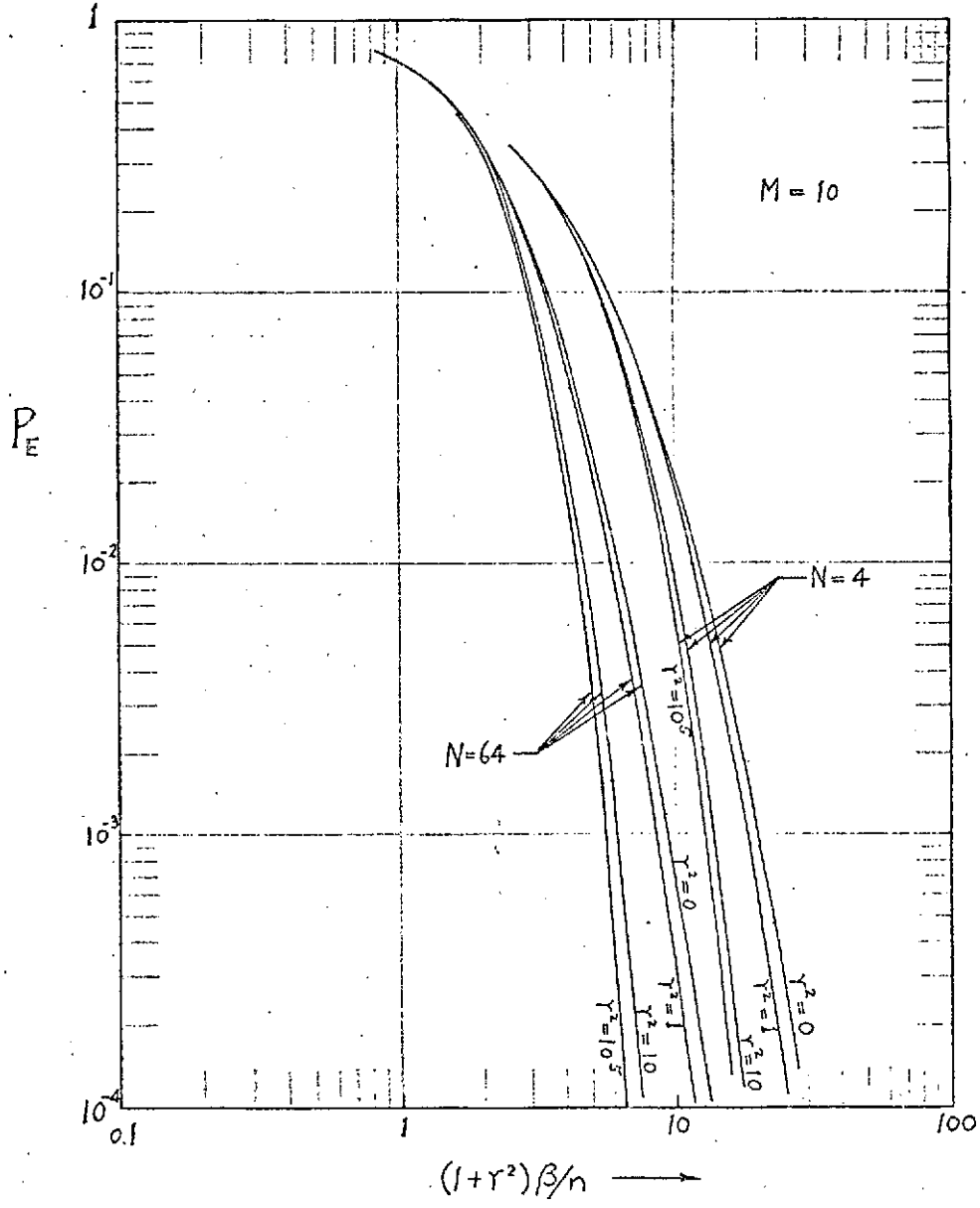

Fig. 8 Word Error Probability of Wideband Noncoherent MFSK Receiver with Multipath Fading (M = 10)

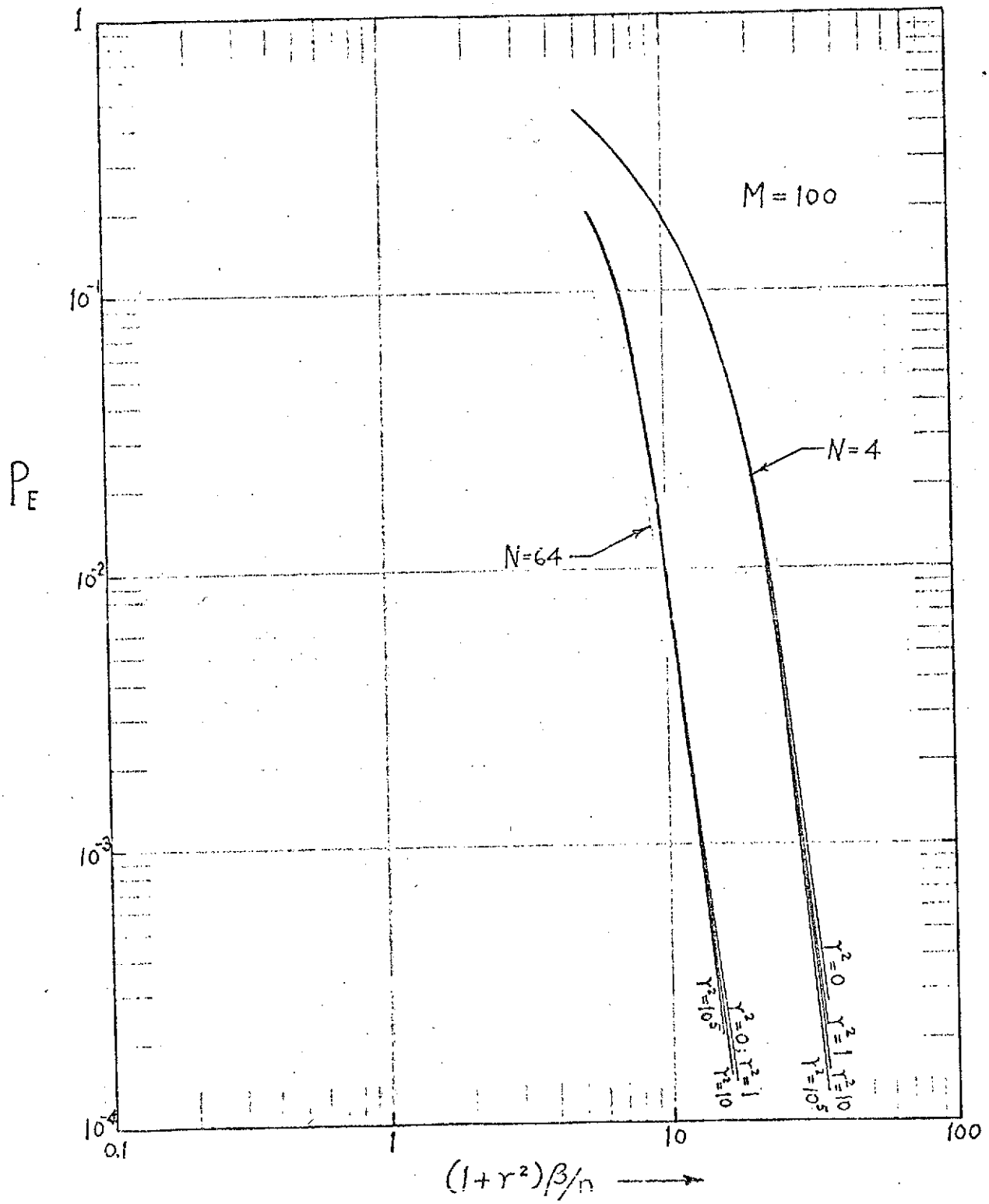

Fig. 9 Word Error Probability of Wideband Noncoherent MFSK Receiver with Multipath Fading (M = 100)

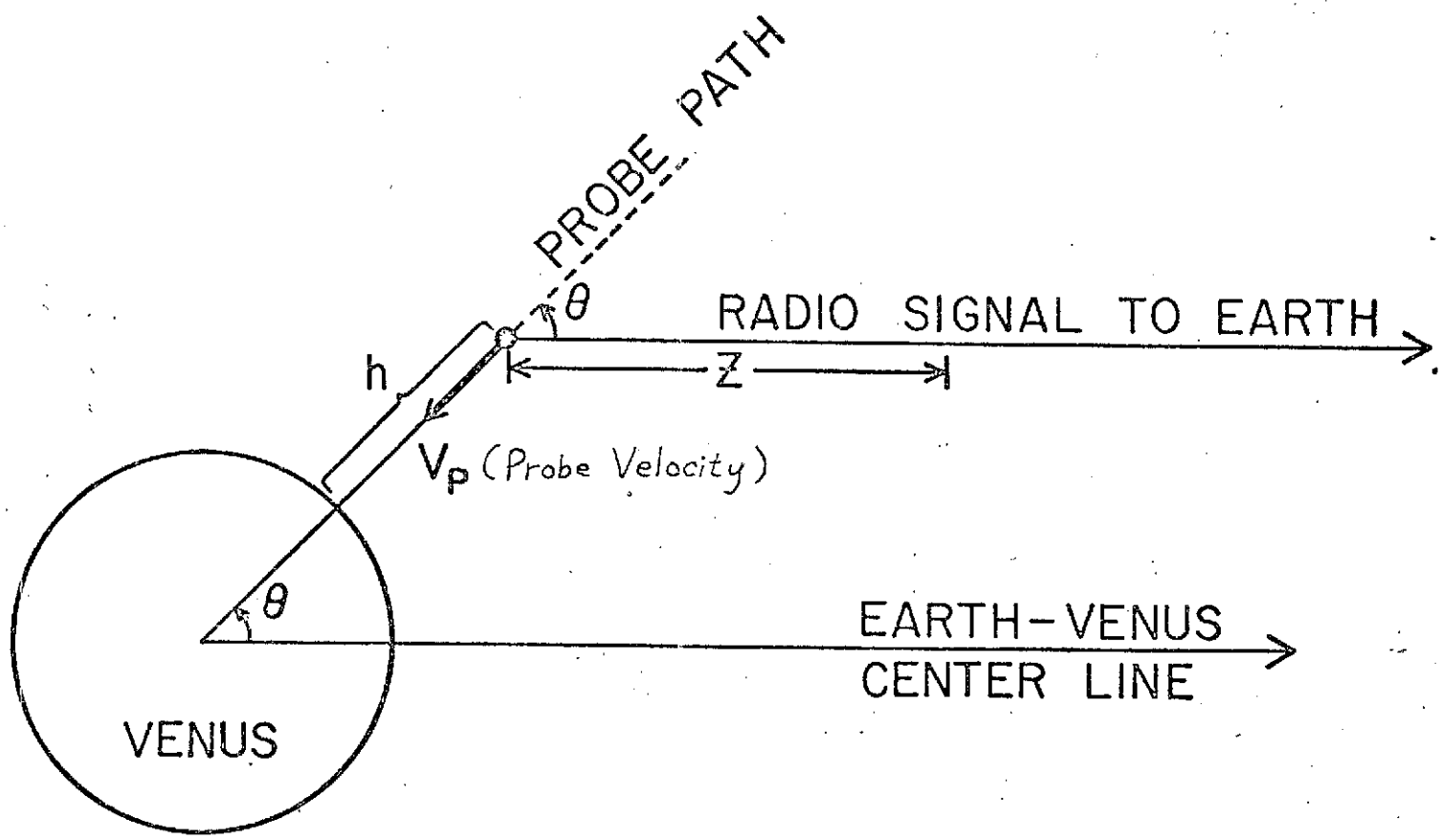

Fig. 10 Geometry of a Venus - Earth Communication Link

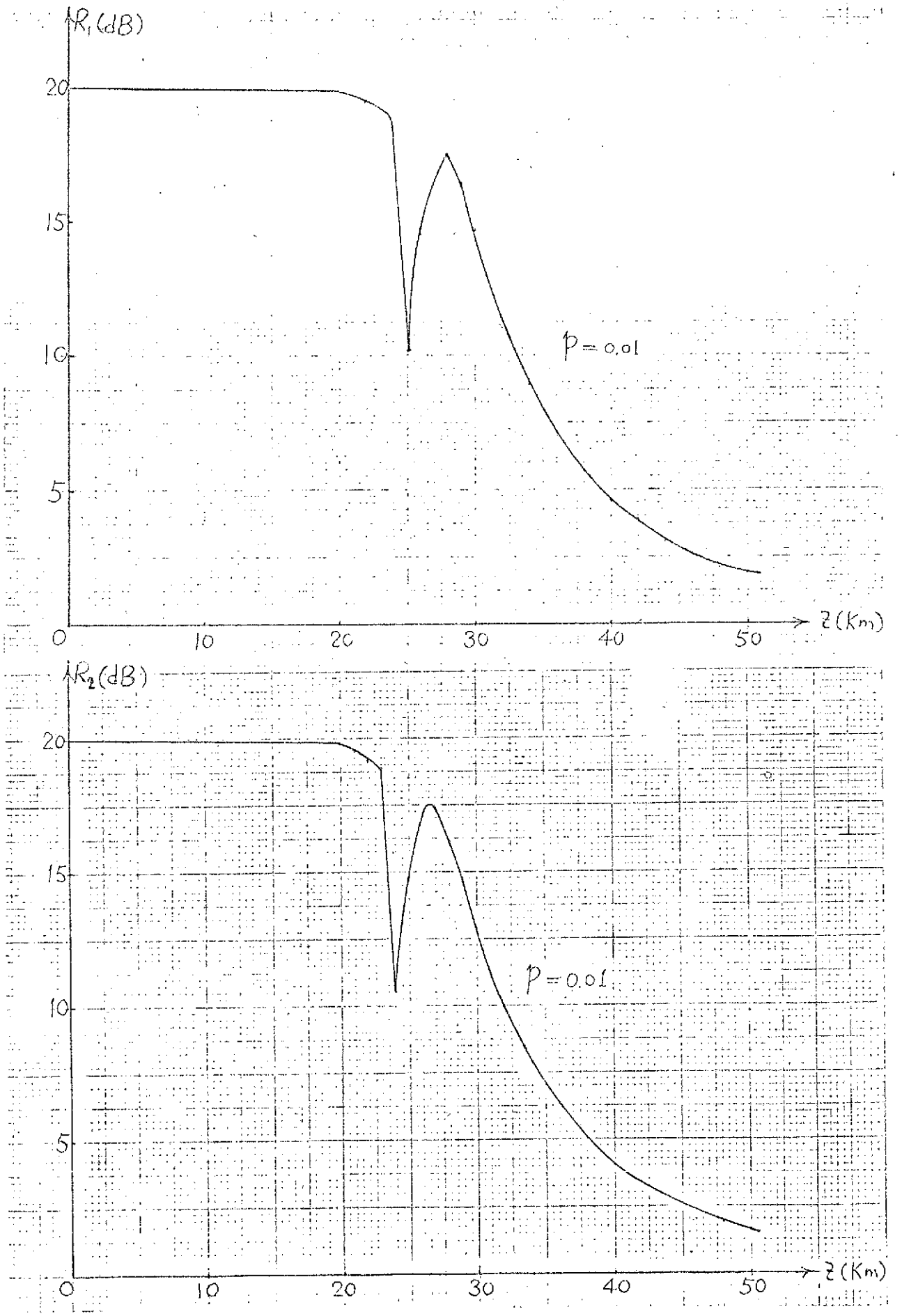

Fig. 11 Fading Level for Small Probability.

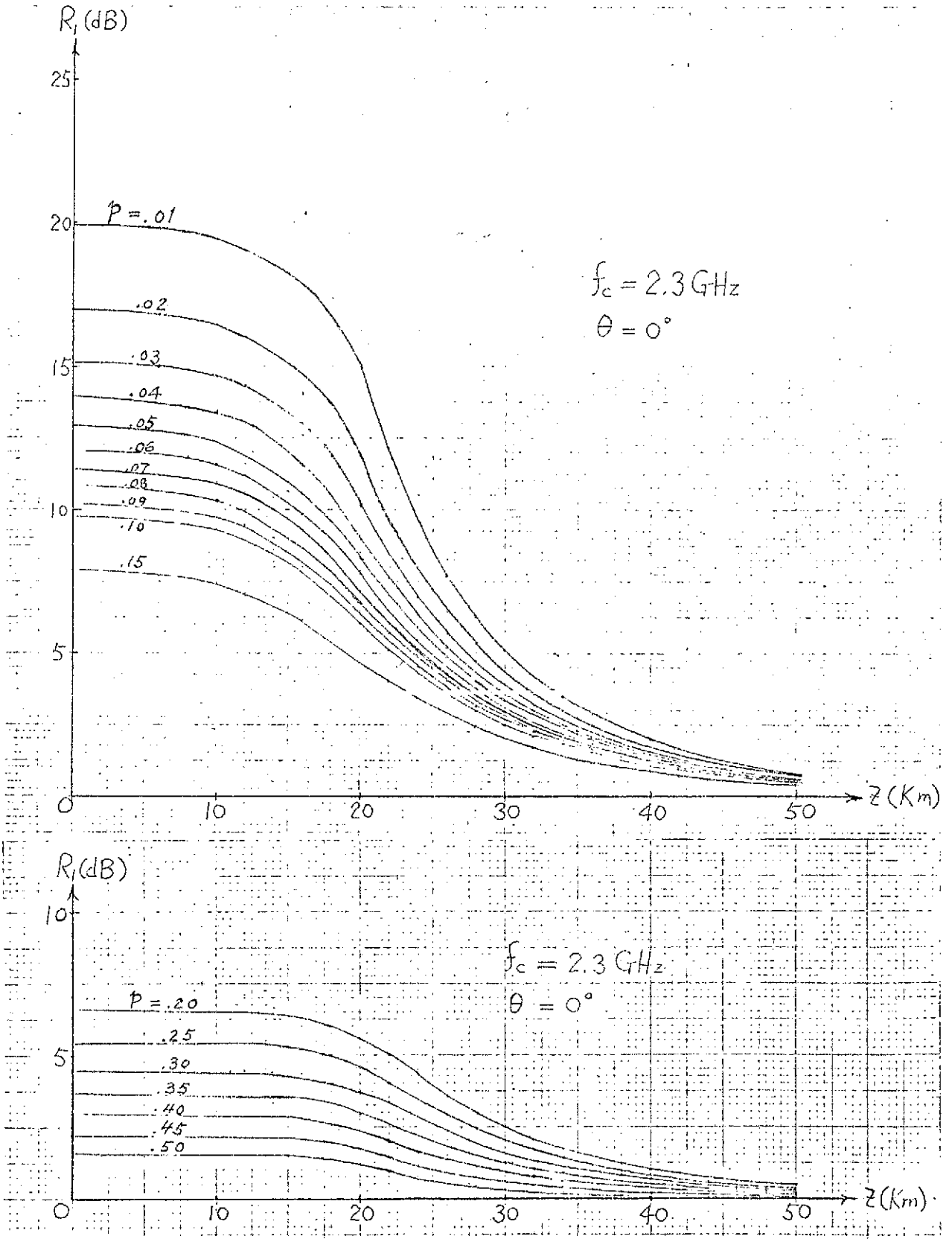

Fig. 12 Fading Level vs Altitude

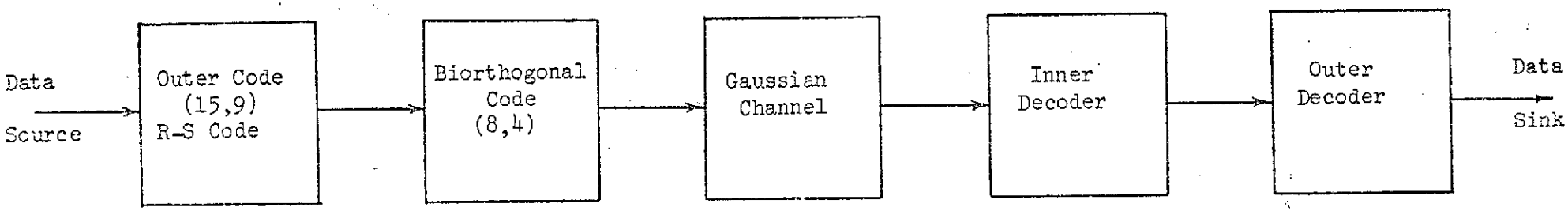
Data
Source
Outer Code
(15,9)
R-S Code
Biorthogonal
Code
(8,4)
Gaussian
Channel
Inner
Decoder
Outer
Decoder
Data
Sink

Fig. 13. Code I

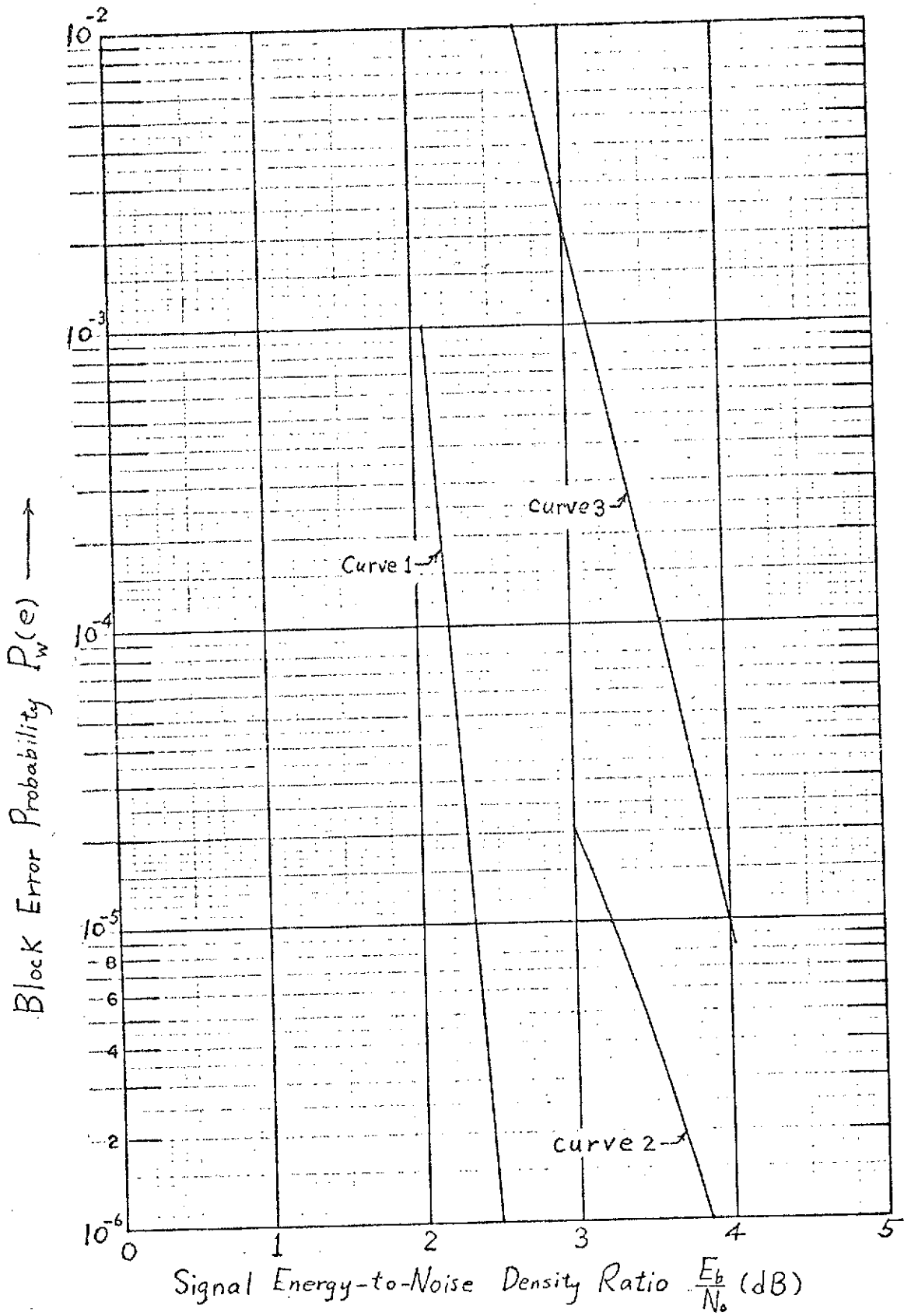

Fig. 14 Word Error Probability of Code I

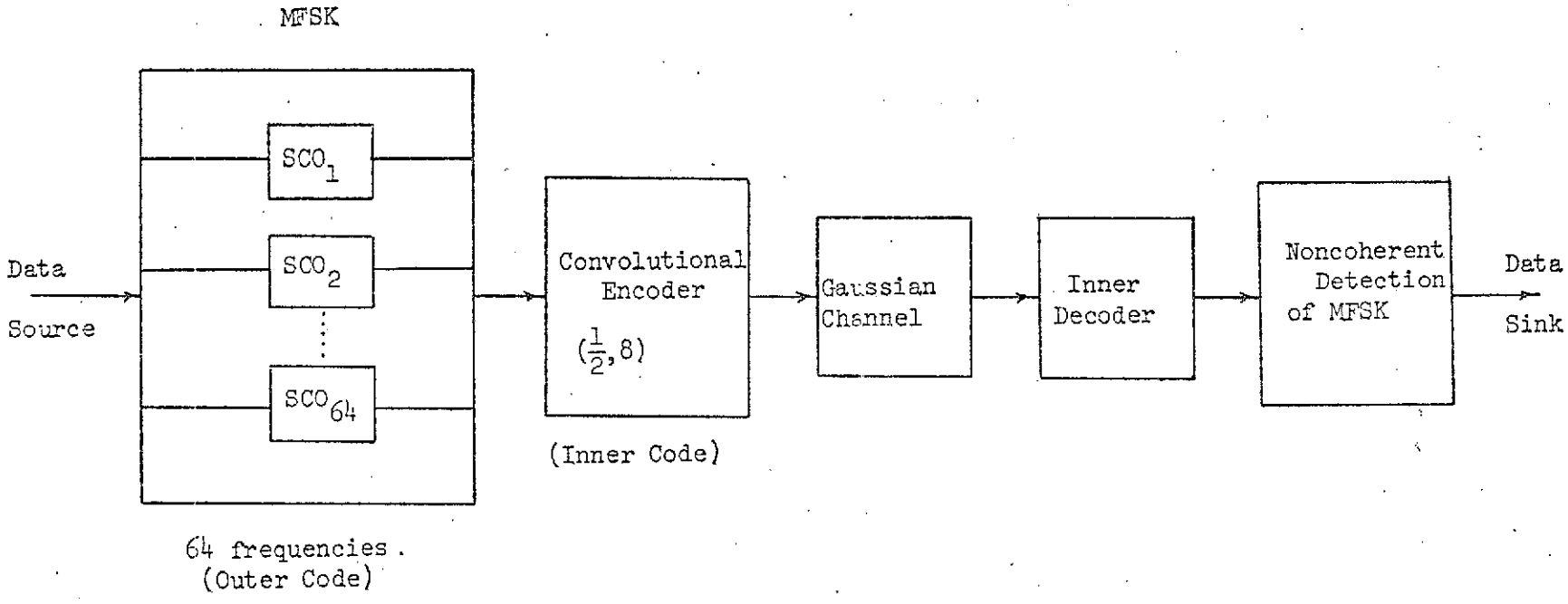

Fig. 15 Code III

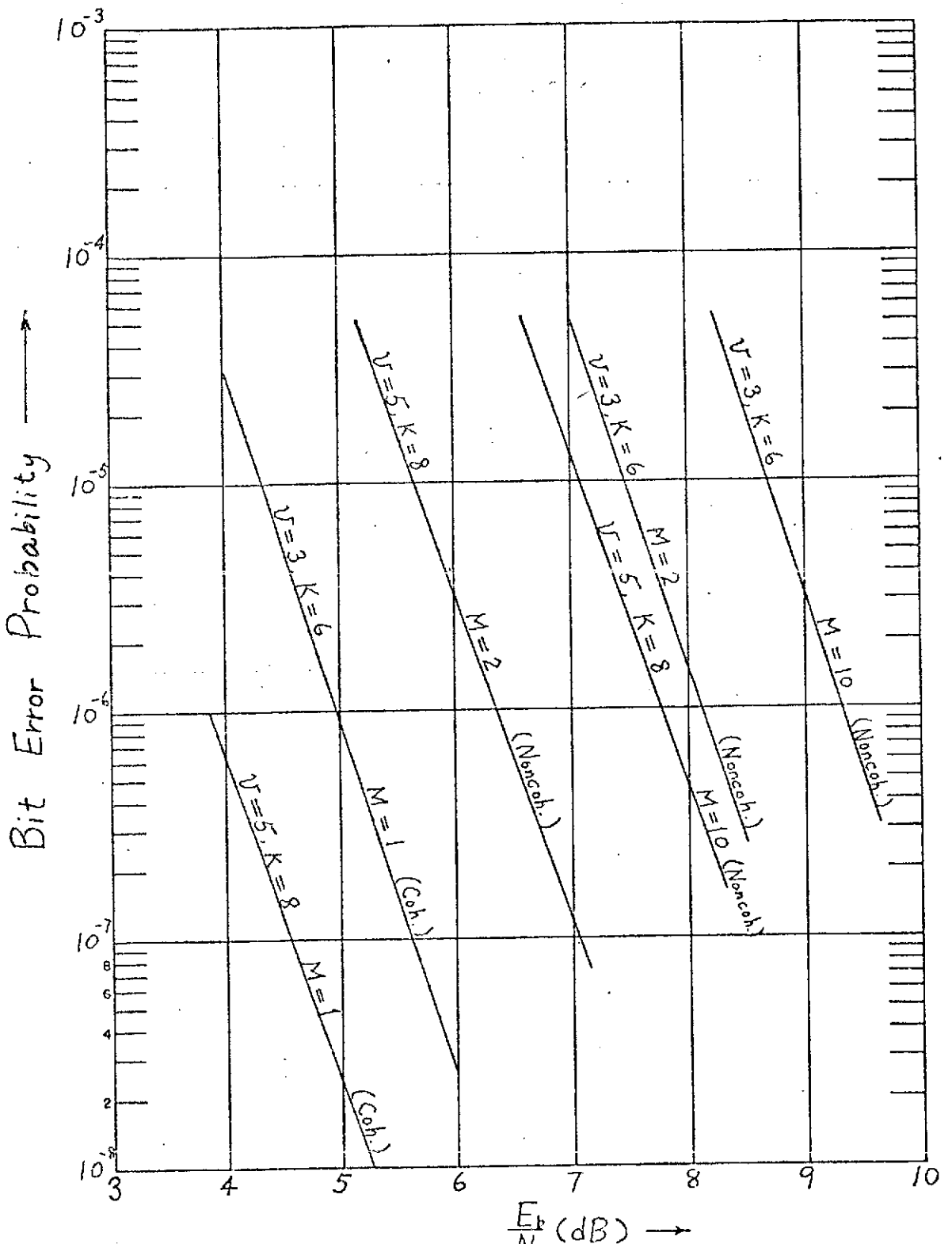

Fig. 16 Bit Error Probability of Code II

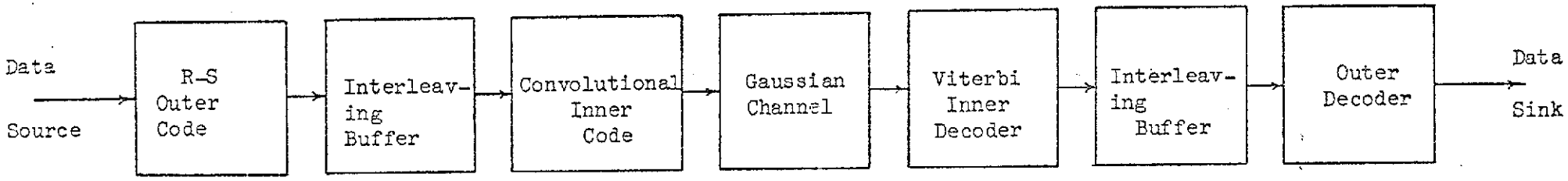

Fig. 17 Code III

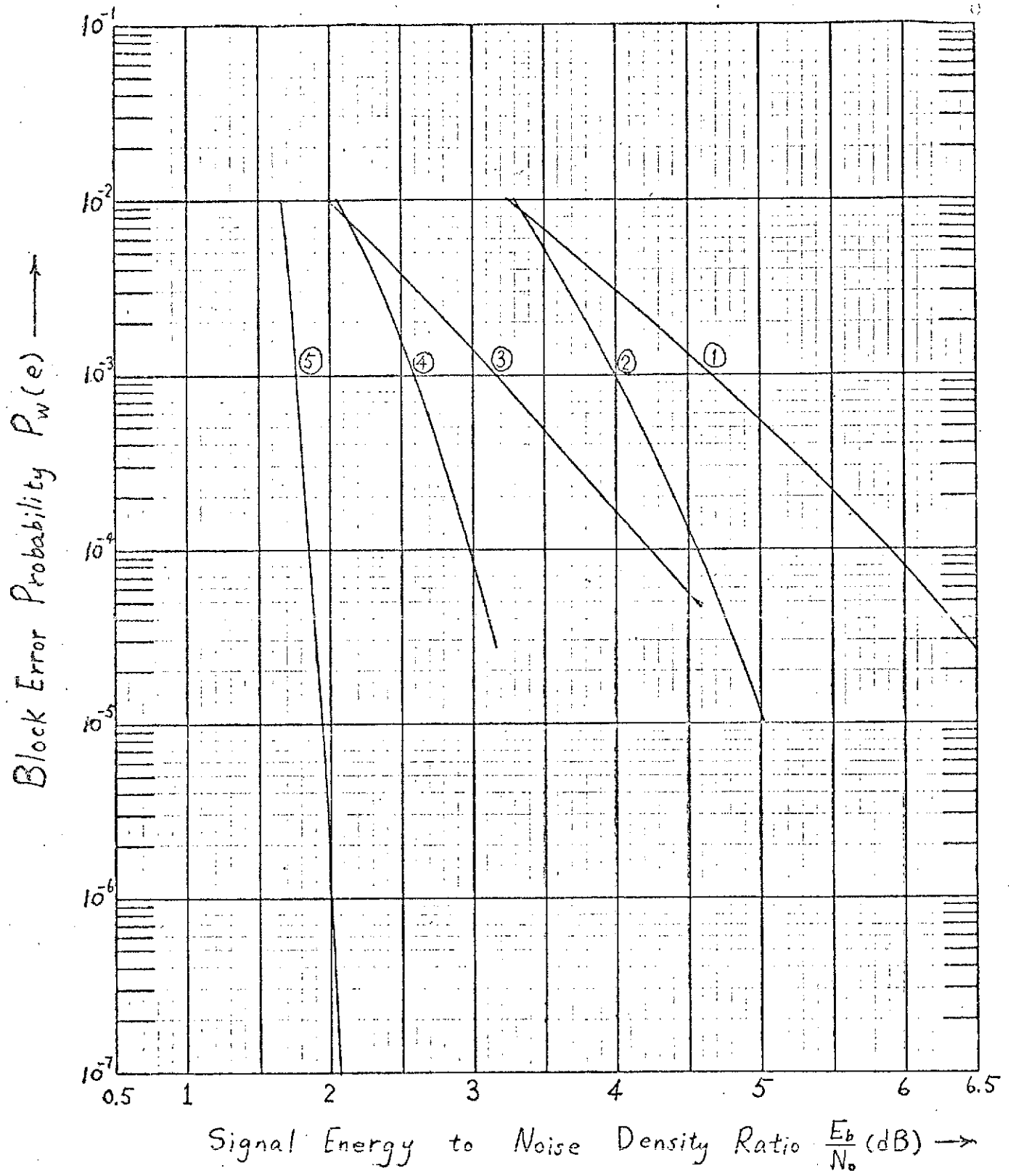

Fig. 18 Word Error Probabilities of Several Coding Techniques: (1) 5-bit Bi-orthogonal Code, (2) (31,25,5) Bi-orthogonal/R-S Code, (3) (1/2,8) Convolutional Code (Viterbi Decoding), (4) (1/2,8) Convolutional/(31,25) R-S Code, and (5) Best Concatenated Code, (1/3,8) Convolutional/R-S Code.

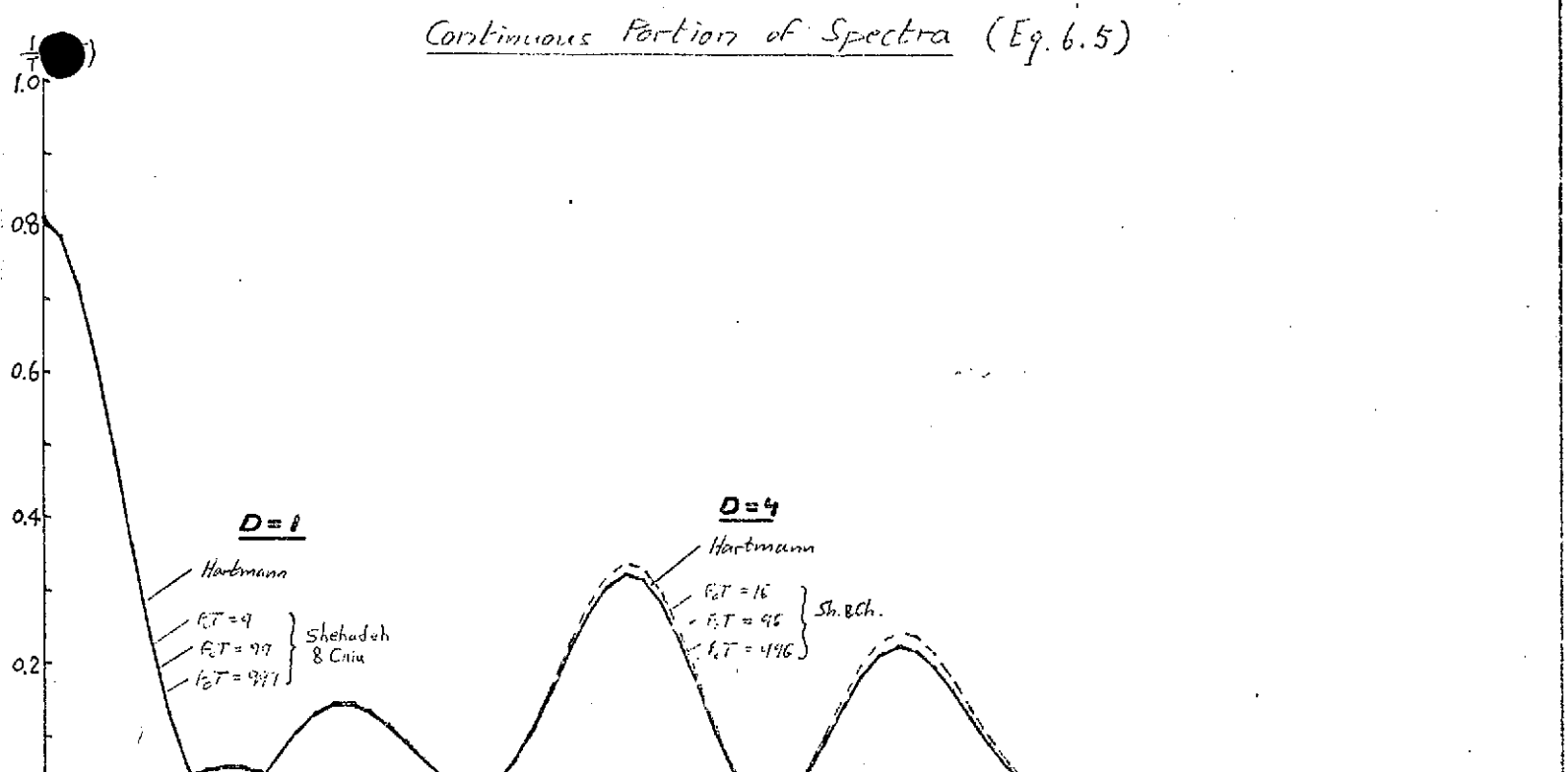
Continuous Portion of Spectra (Eq. 6.5)
1.0
0.8
0.6
0.4
0.2
D = 1
Hartmann
Shehadeh & Chiu
D = 4
Hartmann
Sh. & Ch.
0
1
2
3
4
5
6
7
8
F

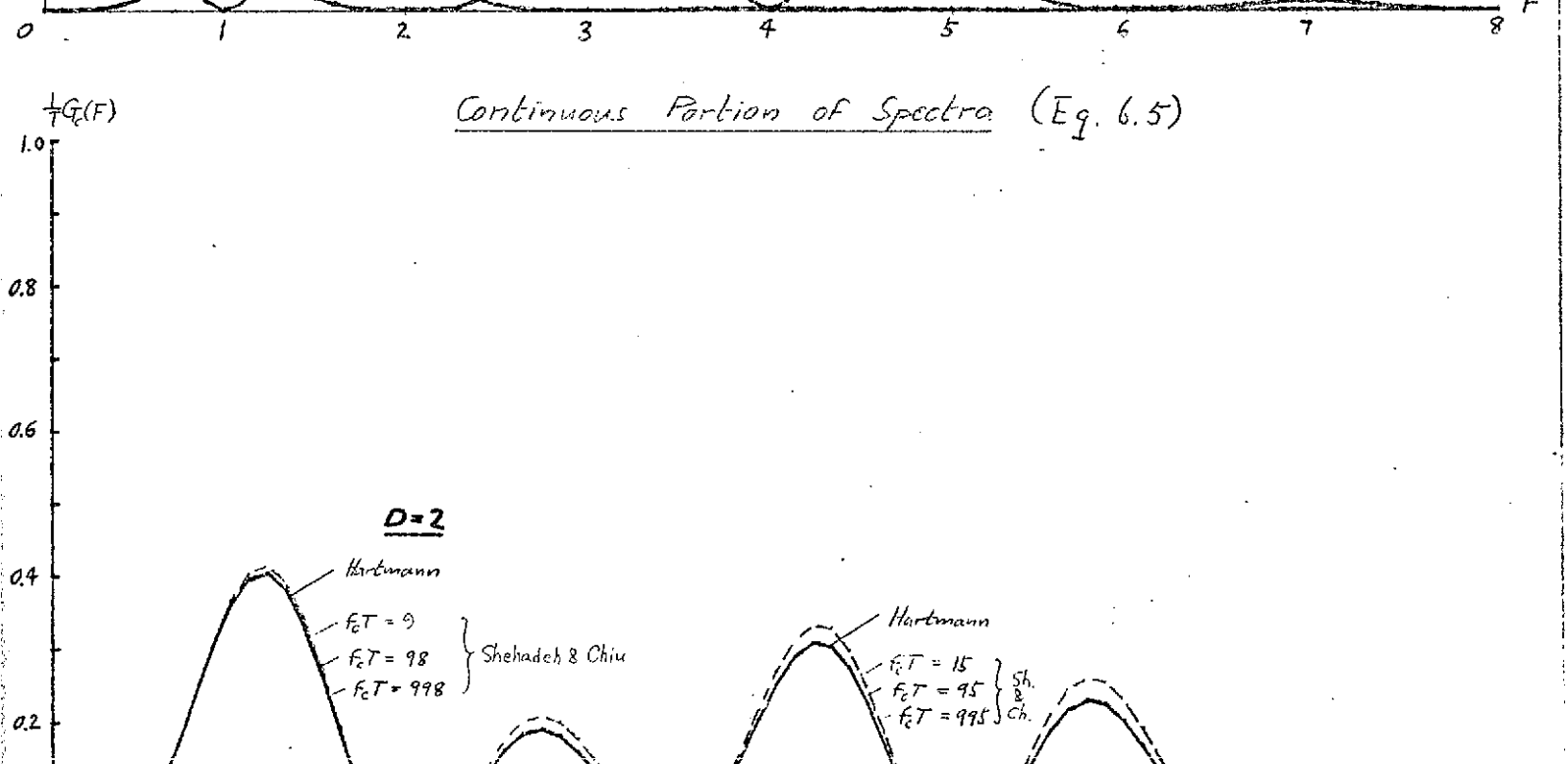
Continuous Portion of Spectra (Eq. 6.5)
1.0
0.8
0.6
0.4
0.2
D = 2
Hartmann
Shehadeh & Chiu
Hartmann
Sh. & Ch.
0
1
2
3
4
5
6
7
8
F

Fig. 19

S.M.U. SYSTEM SUBROUTINE - PLOTIT

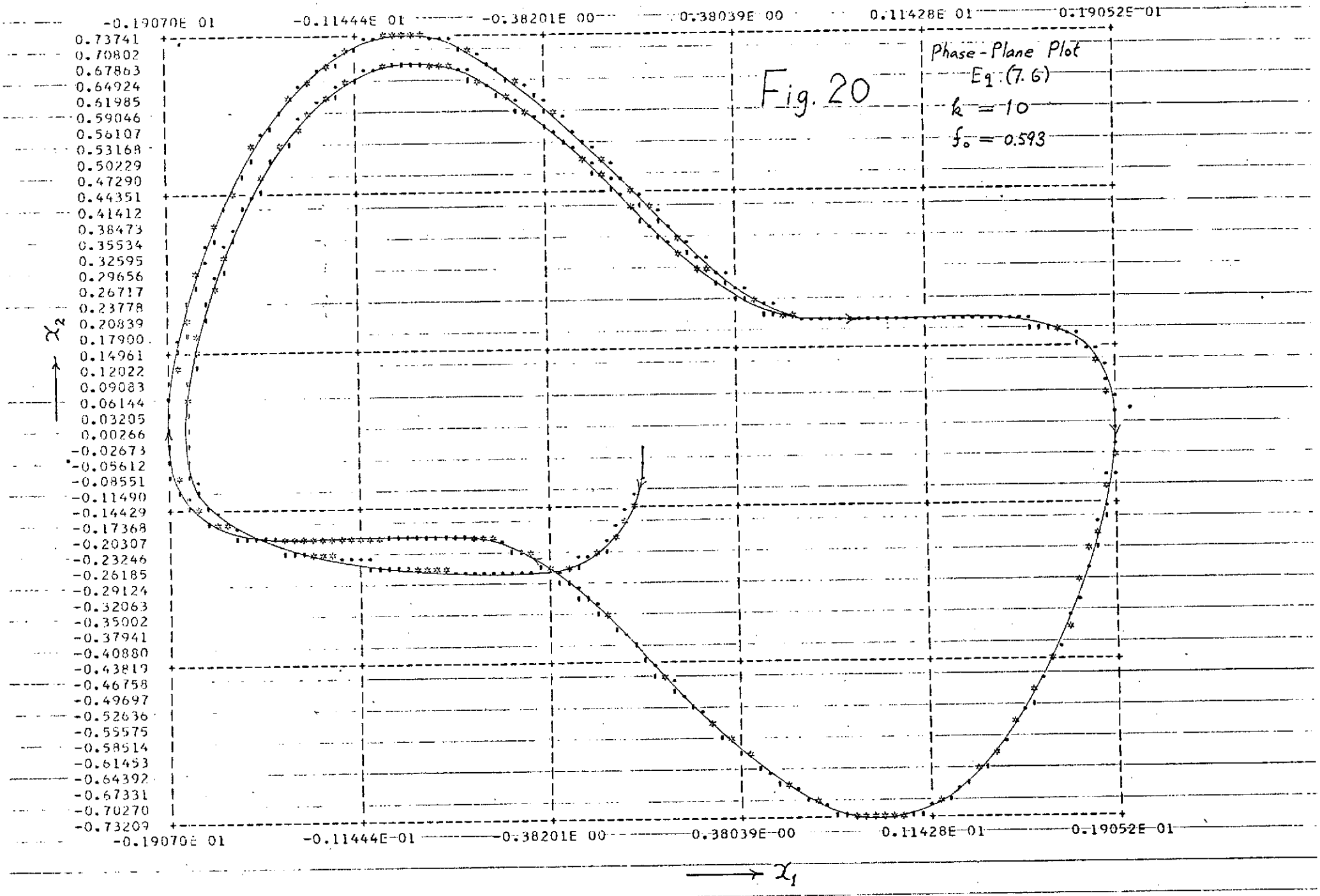

Fig. 20

S.M.U. SYSTEM SUBROUTINE - PLOTIT

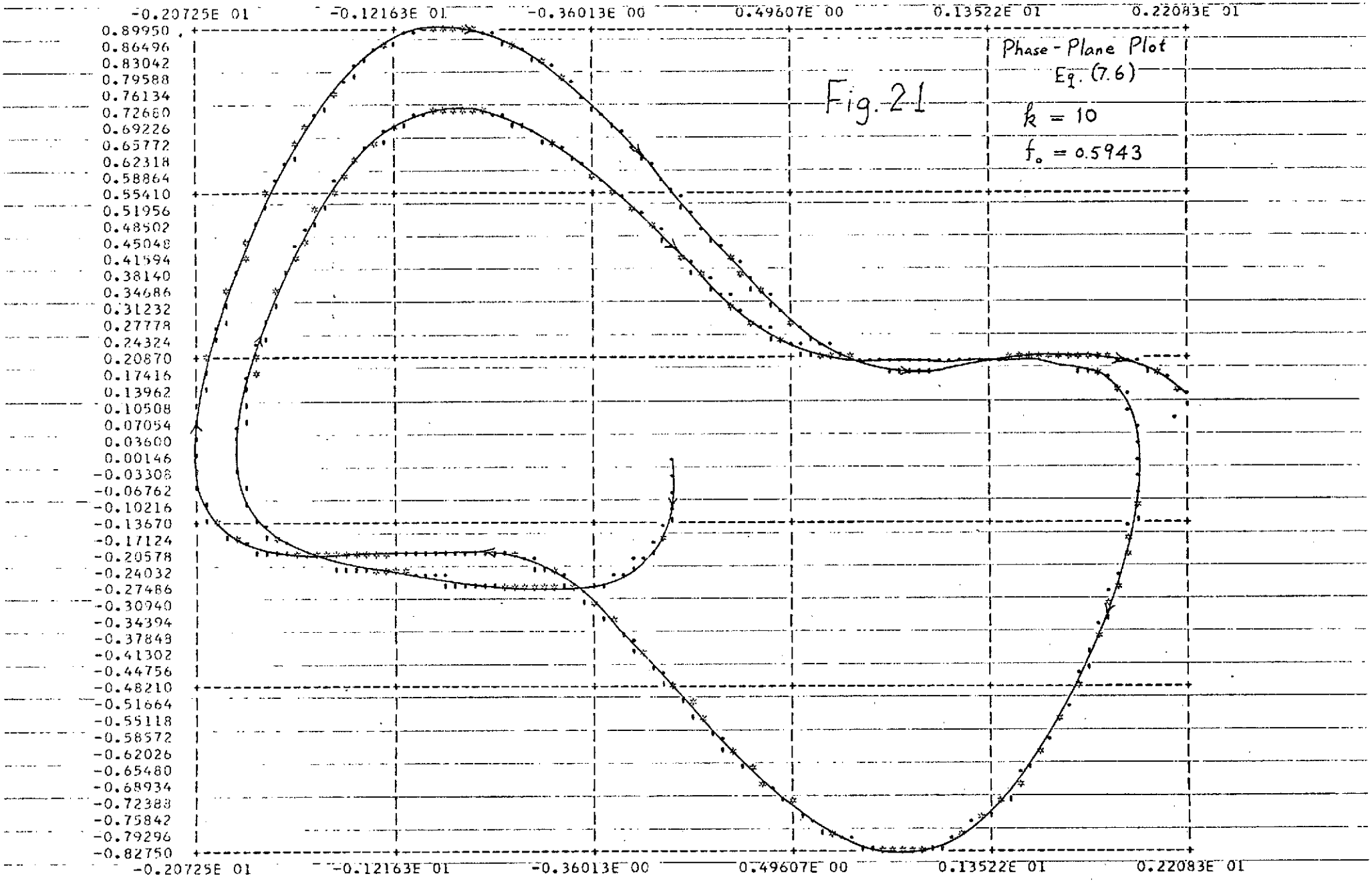

Fig. 21

S.M.U. SYSTEM SUBROUTINE - PLOTIT

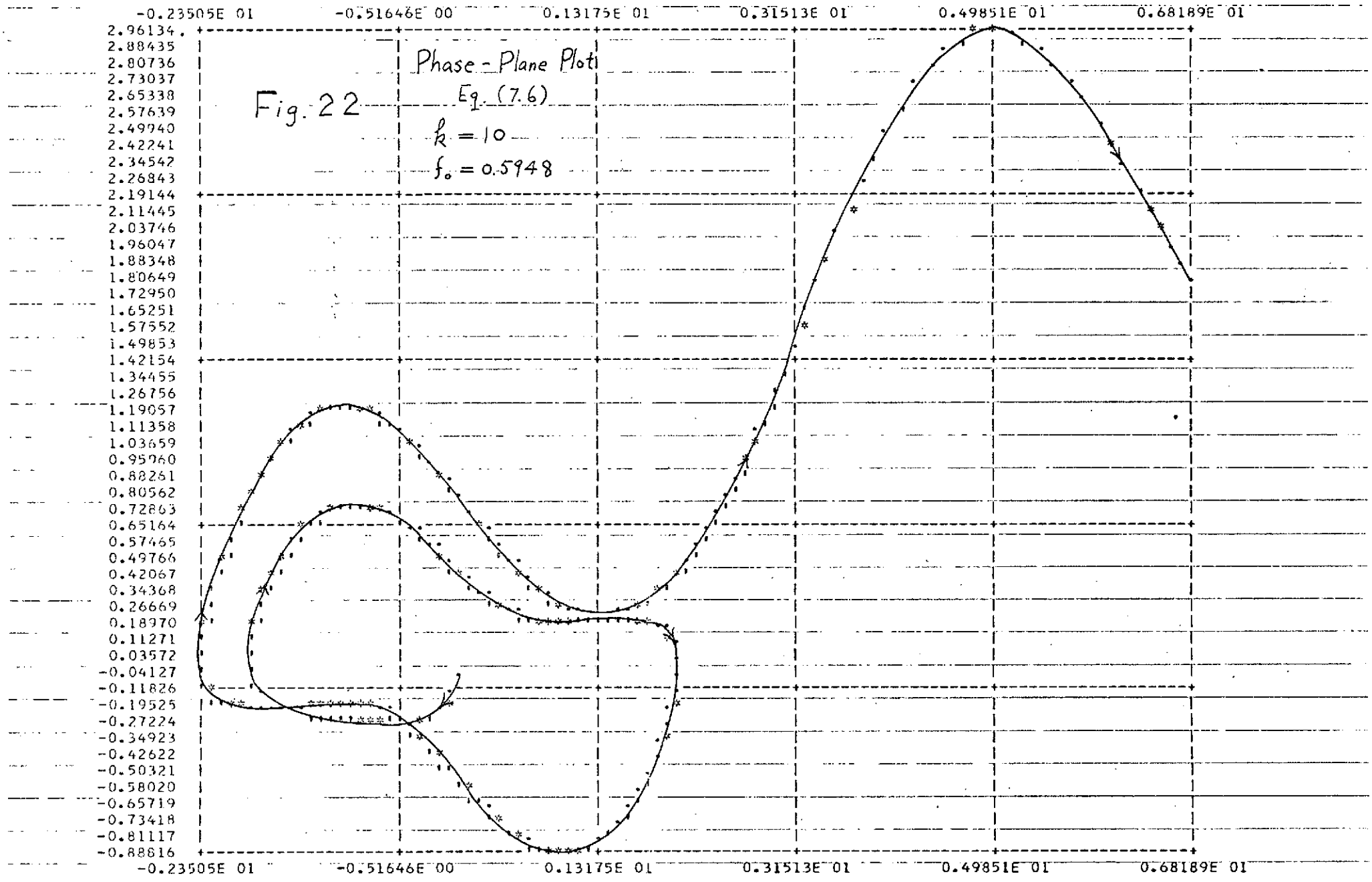

Fig. 22

APPENDIX - CHAPTER 2

MAINPGM

```
      IMPLICIT REAL*8(A-H,O-Z)
      DIMENSION A(1001),B(1001),P(3),X(3)
1     READ(1,10,END=5000)M,NBITS,GMSQ,P(1),P(2),N6,E6,E7,E8,ERROR
10    FORMAT(2I5,F5.0,2D10.0,I5,3F10.0,D10.0)
      M8=M-1
      N=2**NBITS
      N8=N-1
      WRITE(3,20)M,N,GMSQ,N6
20    FORMAT('0M=',I7,5X,'N=',I7,5X,'GMSQ=',F10.4,10X,'WITH',I5,' ORDINA
     ;TES'/'0  P',15X,'X(P) INITIAL'/)
      P(3)=1.-P(1)
      AL9=0.
      IF(M-1)170,170,40
40    DO 50 L=2,M8
      XL=L
50    AL9=AL9+DLOG(XL)
170   DO 200 I=1,3
      P9=P(I)
      C2=P9**(1./N8)
      Z1=M
180   CALL GAMIN(M,M8,Z1,H)
      E1=(H-C2)/DEXP(M8*DLOG(Z1)-Z1-AL9)
      Z1=Z1-E1
      IF(DABS(E1).GE.1.D-6)GO TO 180
      X(I)=Z1
200   WRITE(3,60)P(I),X(I)
60    FORMAT(1X,1P2D15.6)
      WRITE(3,70)
70    FORMAT('0E/N0',15X,'PE(N6/2)',10X,'PE(N6)',11X,'PE',14X,'ERROR'/)
300   R6=NBITS*E6*(1+GMSQ)/(M*GMSQ)
      D9=1.+GMSQ+R6
      B9=(1.+GMSQ)/D9
      A2=M*R6*GMSQ/D9
      H1=(X(3)-X(1))/N6
      N61=N6+1
      DO 630 I=1,N61
      X9=X(1)+H1*(I-1)
      CALL QSUBM(M,A2,X9*B9,ERROR,Q)
      CALL GAMIN(M,M8,X9,H)
      H=N8*(H**(N8-1))
      H=H*DEXP(M8*DLOG(X9)-X9-AL9)
630   A(I)=Q*H
      AI1=0.
      DO 670 I=2,N6,2
670   AI1=AI1+A(I)
      AI1=2.*AI1+.5*(A(1)+A(N61))
      N6M=N6-1
      DO 710 I=3,N6M,2
710   AI1=AI1+A(I)
```

QSUBM

```
      SUBROUTINE QSUBM(M9,A2,B2,E9,Q)
C     COMPUTES THE GENERALIZED Q FUNCTION WHERE
C     M9= M , A2= A**2/2 ,  B2= B**2/2 ,  E9 = ERROR LIMIT,  Q = THE  ANSWER
      IMPLICIT REAL*8(A-H,O-Z)
      XK0=DEXP(-A2)
      D0=DEXP(-B2)
      G0=1.-D0
      IF(E9.GT.1)GO TO 316
      R1=.5+DSQRT(2.*A2*B2)
      Q=1.-G0*XK0
      R=1.
  307 XK0=A2*XK0/R
      D0=B2*D0/R
      G0=G0-D0
      E4=G0*XK0
      Q=Q-E4
      IF(R.LT.R1)GO TO 314
      IF(E4.LT.E9)GO TO 337
  314 R=R+1
      GO TO 307
  316 M8=M9-1
      XM8=M8
      R1=.5*(1.+XM8*(DSQRT(1.+8.*A2*B2/(XM8**2))-1.))
      D3=D0
      DO 10 M7=1,M8
      D3=B2*D3/M7
   10 G0=G0-D3
C     DO 11 M=2,M9
   11 D0=D0*B2/(M-1)
      Q=1.-G0*XK0
      R=1.
  328 XK0=A2*XK0/R
      D0=B2*D0/(R+XM8)
      G0=G0-D0
      E4=G0*XK0
      Q=Q-E4
      IF(R.LT.R1)GO TO 335
      IF(E4.LT.E9)GO TO 337
  335 R=R+1.
      GO TO 328
  337 RETURN
      END
```

GAMIN

```
      SUBROUTINE GAMIN(M9,M8,X9,H5)
C     COMPUTES NORMALIZED INCOMPLETE GAMMA FUNCTION  WHERE
C     M9 = M,   M8=M-1 ,   X9 =X   , H5 = THE ANSWER
      IMPLICIT REAL*8(A-H,O-Z)
      D5=DEXP(-X9)
      H5=1.-D5
      IF(M9.EQ.1)GO TO 287
      DO 286 M=1,M8
      D5=(X9/M)*D5
  286 H5=H5-D5
  287 RETURN
      END
```

```
      AI1=2.*H1*AI1/3.
      AI2=AI1
      DO 770 I=1,N61,2
770   B(I/2+1)=A(I)
      AI1=0.
      N5=N6/2
      DO 820 I=2,N5,2
820   AI1=AI1+B(I)
      AI1=2.*AI1+.5*(B(1)+B(N5+1))

      N5M=N5-1
      DO 860 I=3,N5M,2
860   AI1=AI1+B(I)
      AI1=4.*H1*AI1/3.
      AI8=(AI2-AI1)/15.
      AI3=AI2+AI8
      AI1=1.-AI1
      AI2=1.-AI2
      AI3=1.-AI3
      AI8=-AI8
      WRITE(3,90)E6,AI1,AI2,AI3,AI8
90    FORMAT(1X,1P5D15.6)
      E6=E6+E8
      IF(E6-E7)300,300,1
5000  CALL EXIT
      END
```

APPENDIX - CHAPTER 4

MAINPGM

```
C     TITLE : AMPLITUDE FADING STATISTICS --- AFS-1.
C ***************************************************************************
C
C     THIS PROGRAM CALCULATES THE FADING LEVELS FOR DIFFERENT
C     PROBABILITIES AS A FUNCTION OF ALTITUDE ABOVE THE VENUS SURFACE.
C     FOR EACH PROBABILITY INPUT, THE OUTPUT CONSISTS OF THE FADING
C     LEVELS IN DB AS A FUNCTION OF THE ALTITUDE--Z. THE VALUES 'R1' AND
C     'R2' ARE THE FADING LEVELS COMPARED TO FREE SPACE FOR TWO DIF-
C     FERENT SCALING LAWS.
C
C     IN THIS PROGRAM THE EXPRESSIONS FOR K1 AND K2 ARE BASED ON SOME
C     FORMULARS BY DE WOLF.
C
C     FREQUENCY = 2.3GHZ,  THATA = 0 DEGREE.
C
C ***************************************************************************
      REAL K1,K2,K
1     FORMAT(F20.3)
2     FORMAT(5X,F12.9,4(F14.5,3X))
3     FORMAT(' P=',5X,F4.2)
4     FORMAT(10X,'Z(KM)',10X,'R1(DB)',10X,'R2(DB)',10X,'K1',14X,'K2')
5     FORMAT('0')
10    READ(1,1,END=300)P
      WRITE(3,5)
20    WRITE(3,3) P
      WRITE(3,4)
30    CALL SUB1(YY,P)
40    P=1.-P
50    DO 190 I=1,51
      Z=I-1.
60    H=1./.0785
70    E=EXP(-Z/H)
80    S1=2.87*E
90    S2=1.95*E
100   K1=SQRT(EXP(2.*S1**2)-1.)
110   K2=SQRT(EXP(2.*S2**2)-1.)
120   K=K1
130   CALL SUB2(R,K,YY,P)
140   R1=R
150   K=K2
160   CALL SUB2(R,K,YY,P)
170   R2=R
1     WRITE(3,2) Z,R1,R2,K1,K2
190   CONTINUE
200   GO TO 10
300   CALL EXIT
      END
```

```
      SUBROUTINE SUB1(YY,P)
C *****************************************************************************
C
C     SUBROUTINE TO FIND Y, WHERE Y IS THE LEVEL SUCH THAT FOR A GAUS-
C     SIAN OR NORMAL PROBABILITY DISTRIBUTION, P=PROB(R'<Y)
C
C *****************************************************************************
  970 Q=1.-P
  980 IF(Q.GT..5) GO TO 1050
  990 A=1.
 1000 T=SQRT(ALOG(1./Q**2))
 1010 Y=2.515517+T*(0.802853+0.010328*T)
 1020 Y=Y/(1.+T*(1.432788+T*(0.189269+0.001308*T)))
 1030 Y=A*(T-Y)
      YY=Y
 1040 GO TO 1080
 1050 A=-1.
 1060 Q=1.-Q
 1070 GO TO 1000
 1080 RETURN
      END
      SUBROUTINE SUB2(R,K,YY,P)
C *****************************************************************************
C
C     SUBROUTINE TO CALCULATE THE FADING LEVEL IN DB COMPARED TO THE
C     FREE SPACE LEVEL. THE CALCULATION IS BASED ON THE NORTON'S EQUA-
C     TIONS.
C
C *****************************************************************************
      REAL K,K8,LOG
      LOG(AA)=ALOG(AA)
      Y=YY
  650 IF(K.GT.1.) GO TO 800
  660 K8=K**2
  670 IF(K.GT..1) GO TO 720
  680 R=K*Y/1.414*(1.-3./8.*K8)+K8/4.*(1.-K8/6.)
  690 R=8.68589*(R-(K*Y)**2*(1./4.-K*Y/6./1.414))
  700 R=R-3.68589*LOG(SQRT(1.+K8))
  710 GO TO 940
  720 R=1.+K8/4.*(1.-K8/24.*(1.-.35*K8))
  730 R=R+Y*K/1.414*(1.-K8/8.*(1.-3./16.*K8))
  740 R=R+Y**2*K8**2/24.*(1.-17./40.*K8)
  750 R=R-K**5*Y**3/32./1.414+K**6*Y**4/80.
  760 R=8.68589*LOG(R)
  770 R5=8.68589*LOG(SQRT(1.+K8))
  780 R=R-R5
  790 GO TO 940
  800 X=-LOG(P)
  810 IF(K.GT.10.) GO TO 900
  820 K8=1./(K**2)
  830 R=1.+K8*(1.+.5*K8*(1.-X/2.)+K8**2/6.*(1.-2.5*X+2./3.*X**2))
  840 R=R+(K8**4)/24.*(1.-17./2.*X+49./6.*X**2-33./24.*X**3)
  850 R=K**2*X*R
  860 R=4.3429*(LOG(R))
      R5=8.68589*LOG(SQRT(1.+K**2))
      R=R-R5
  890 GO TO 940
  900 R=8.68589*LOG(K)+4.3429*LOG(X)
  910 R=R+4.3429/(K**2)*(1.-X/4./(K**2))
  920 R5=8.68589*LOG(SQRT(1.+K**2))
  930 R=R-R5
  940 RETURN
      END
```

APPENDIX - CHAPTER 7

MAINPGM

```
C*****************************************************
C     PHASE PLANE ANALYSIS WITH PERFECT FILTER    *
C*****************************************************
      REAL K
      DIMENSION Y(1000),Z(1000),TAU1(1000),DTAU1(1000)
      DIMENSION FO(2)
      DATA FO/.594,.5945/
      H=.05
      W=2./3.
      R=H/(2.*W)
      PI=3.14159265
1     FORMAT(4F5.2)
2     FORMAT(1HO,3X,'NUMBER',21X,'X1',24X,'X2',22X,'DTAU',20X,'TAU')
3     FORMAT(5X,I4,17X,E14.7,13X,E14.7,12X,E14.7,9X,E14.7)
4     FORMAT(1H1)
5     FORMAT(1HO)
6     READ(1,1,END=10)X1A,X2A,A,B
      DO 9 J=1,2
      K=10.
      AP=B/A
      FREQ=FO(J)
      WZ=2.*PI*FREQ
      X1=X1A
      X2=X2A
      TAU=0.
      DTAU=0.
      X1D=X2
      X2D=-COS(X1)*X2-AP*SIN(X1)-(K*(WZ**2)/(A**2))*SIN((WZ*TAU/A)+PI/6.
     &)
      DO 8 I=1,1000
      IF(I.LE.2)GO TO 7
      DTAU=ABS((Y(I-1)-Y(I-2))/((Z(I-1)+Z(I-2))/2.))
      TAU=TAU+DTAU
7     X1H=X1+R*X1D
      X2H=X2+R*X2D
      X1DH=X2H
      X2DH=-COS(X1H)*X2H-AP*SIN(X1H)-(K*(WZ**2)/(A**2))*SIN((WZ*TAU/A)+P
     &I/6.)
      X1=X1+H*((1.-W)*X1D+W*X1DH)
      X2=X2+H*((1.-W)*X2D+W*X2DH)
      X1D=X2
      X2D=-COS(X1)*X2-AP*SIN(X1)-(K*(WZ**2)/(A**2))*SIN((WZ*TAU/A)+PI/6.
     &)
      Y(I)=X1
      Z(I)=X2
      TAU1(I)=TAU
      DTAU1(I)=DTAU
8     CONTINUE
      CALL PLOTIT (Y,Z,1000)
      WRITE(3,4)
      WRITE(3,2)
9     CONTINUE
10    CALL EXIT
      END
```